PAPER

Check for updates

Good practices for reporting the photocatalytic evaluation of a visible-light active semiconductor: Bi₂O₃, a case study†

Agileo Hernández-Gordillo, [iD] ‡[a] Monserrat Bizarro, [iD] [a] Tanveer A. Gadhi, [iD] [b] Ana Martínez, [a] Alberto Tagliaferro [iD] [cd] and Sandra E. Rodil [iD] *[a]

In this paper, we discuss the importance of distinguishing the contributions of photolysis, adsorption, sensitization, degradation and mineralization processes to the photocatalytic activity of a visible-light active semiconductor: Bi₂O₃. Based on this case study, we propose a follow-up work plan to obtain the relevant information and achieve proper interpretation of reported data to adequately infer the photocatalytic activity of the Bi₂O₃ material. To do so, we compared the changes in the theoretical and experimental absorbance spectra of three different dyes during the photodegradation process: rhodamine-B (RhB), acid blue 113 (AB) and indigo carmine (IC). Photocatalytic degradation of these dyes using the same semiconductor material (Bi₂O₃) was performed using the standard spectrocolorimetric method while taking care to appropriately consider the competing processes mentioned above. Furthermore, the degree of mineralization achieved due to the photocatalytic degradation of the dyes was obtained using the total organic carbon (TOC) analysis. The commonly used evaluation of the results suggests that a certain degree of photodegradation and mineralization was achieved. However, careful analysis indicates that this was mainly due to a decrease in the relative concentration of the dye molecules in the solution because of their adsorption on the surface of the semiconductor and not to complete degradation.

Introduction

Heterogeneous visible-light photocatalysis is becoming an important alternative for the decomposition of recalcitrant organic pollutants in water, such as phenols, surfactants, dyes, and organic pesticides as well as emergent pharmaceutical and personal care products. Heterogeneous photocatalysis exploits light for the activation of a photocatalytic material that enables oxidation/reduction reactions through the generation of reactive oxygen species (ROS), leading to degradation or complete mineralization of organic pollutants.[1,2] An important goal to achieve during heterogeneous photocatalysis is the mineralization, *i.e.*, the degradation of the parent pollutant and its intermediate products to CO_2 and H_2O without

any residual contaminants.[3,4] When this mineralization process can be carried out using solar light, heterogeneous visible-light photocatalysis becomes a viable and sustainable alternative for water treatment. Hence, there is worldwide interest in the development of new or modified photocatalytic materials which are photoactive under visible light illumination to take full advantage of the solar spectrum.[5–8]

Regarding dyes, it has been reported that approximately 1% to 15% of synthetic textile dyes are discharged in wastewater streams.[9,10] The discharge of colored effluent obstructs light penetration, disrupting biological processes. Many dyes are harmful to organisms and may cause direct destruction of aquatic species.[11] Therefore, the removal of dyes from industrial wastewater is a major environmental issue. It is hence compulsory to put effort toward the development of new technologies to achieve the elimination of dyes before wastewater discharge. By using UV-active photocatalytic materials, such as TiO_2 and ZnO, it has been clearly demonstrated that different organic dyes can be converted into non-toxic and colorless products, achieving complete mineralization in some cases (CO_2 and water byproducts).[12–14] However, the quest for visible-light active photocatalytic materials capable of degrading organic dyes is not yet complete. One reason is that the ideal photocatalytic material should have an optimum band gap ($E_g < 3$ eV), but at the same time, it should

[a] *Instituto de Investigaciones en Materiales, Universidad Nacional Autónoma de México, Circuito Exterior SN, Ciudad Universitaria, CP 04510, Coyoacán, Cd. De México, Mexico. E-mail: srodil@unam.mx*
[b] *U.S. Pakistan Center for Advanced Studies in Water (USPCASW), Mehran, University of Engineering and Technology, Jamshoro 76062, Pakistan*
[c] *Department of Applied Science and Technology, Politecnico di Torino, Italy*
[d] *UOIT, Canada*
† Electronic supplementary information (ESI) available: Synthesis, characterization and optical properties of the tested semiconductor material. See DOI: 10.1039/c9cy00038k
‡ Present Address: CONACYT Research Fellow.

fulfill the thermodynamic conditions that allow the fast generation of ROS.[15] Moreover, the evaluation of the photocatalytic activity of the material is not as easy as it appears because there are several parameters that must be properly considered, such as solution pH, stirring rate, dissolved oxygen, and dye concentration. We consider that relevant data and discussion about processes that occur during photocatalysis are usually disregarded in many published papers. Identification of processes such as (i) photodiscoloration due to adsorption or photolysis, (ii) dye self-sensitization, (iii) actual photodegradation with the unavoidable formation of intermediate products, and (iv) mineralization of the intermediate products is significant for the correct interpretation of the photocatalytic activity of a semiconductor.

Currently, it is very common to evaluate the photocatalytic activity of "new" photocatalytic materials (nanostructures or thin films) using colored dye solutions as probe pollutants to degrade because the kinetics of the degradation process can be easily followed using a spectrophotometric technique,[16] assuming that the absorbance is solely proportional to the relative dye concentration. However, the simplicity of this quantitative technique has led to false results or incorrect interpretations; this has raised valid criticism by the specialized community,[3,15,17–19] who insist on the importance of understanding the correlation between photocatalysis and heterogeneous catalysis. One important point to consider is that the whole absorbance spectrum of the dye solution should be acquired from UV to visible wavelengths as a function of the irradiation time, rather than only determining the absorbance at a fixed wavelength. Moreover, for dyes, it has been shown that color removal (decoloration, discoloration or decolorization) is not equivalent to dye mineralization; indeed, total color removal can be achieved without mineralization.[12,20] It has also been established that the results obtained from specific semiconductor-dye couples cannot be generalized to other organic molecules, not even to other dyes; this is due to possible synergistic reactions established between the particular dye molecule and the semiconductor, such as sensitization.[14] However, we consider that sensitization and other common misinterpretations of results are not unique to the use of dye solutions but are inherent to the spectrophotometric evaluation of probe solutions using supernatants or aliquots.

In this paper, we propose a methodology consisting of a number of fundamental steps for the photocatalytic evaluation of visible-light active photocatalytic materials; this methodology is applicable to different organic molecules, including dyes. By following the proposed methodology, which includes steps for the determination of certain competing processes occurring during evaluation under dark and illumination conditions, we show that it is possible to reach more reliable conclusions about the photocatalytic activity of a material. Some of the proposed key experiments are already included in many papers; however, good interpretation of the results has not necessarily been provided in all cases, leading to false assessments. The follow-up methodology is supported by experiments using a candidate semiconductor (Bi$_2$O$_3$) and three different dyes. We also performed quantum chemical calculations of the absorbance spectra of the dyes, their intermediates or degradation products and their photobleaching processes. The procedure that we propose for the analysis of photocatalytic activity can be used for any semiconductor material and/or probe molecule.

Experimental and theoretical procedures

The follow-up methodology includes spectrophotometric evaluation of the dye concentration (C_n) measured for each process, namely photolysis (C_{photo}), adsorption (C_{ads}), sensitization (C_{sen}), photobleaching (C_{blea}), and photodegradation (C_{deg}); finally, we propose that a non-spectrophotometric technique should be used to determine the degree of mineralization (% Mine) of the intermediate products in solution. In this case, we present data on mineralization obtained using measurements of the change in the total organic carbon content (TOC).

a) Dye solutions

Three dyes were selected: the cationic dye rhodamine-B (RhB), with a concentration of 5 mg L^{-1}, and the anionic dyes indigo carmine (IC) and acid blue 113 (AB), with concentrations of 10 mg L^{-1} at pH 6.6 ± 0.2, close to the neutral value. For the AB dye, an additional solution was adjusted to an alkaline pH close to 9.5 using drops of NaOH. For each experiment, 10 mg of the α/β-Bi$_2$O$_3$ powder sample (see the ESI,† for synthesis and characterization details) were added to 15 mL of the dye solution, leading to a photocatalyst load of 0.67 g L^{-1}. The stirring rate was kept constant at 1200 rpm while exposing the solution to air to allow oxygen diffusion. The experiments were performed under irradiation of a 9 W UV lamp (irradiating in the wavelength range of 350 to 400 nm) with an irradiance of 27 W m^{-2} and a 9 W white lamp (irradiating in the wavelength range of 420 to 640 nm) with an irradiance of 33 W m^{-2}.[21]

b) Spectrophotometric experiments

The whole absorbance spectra of the dye solutions in the dark and during illumination were measured using a Shimadzu 1800 UV-vis spectrophotometer in the wavelength range from 200 to 800 nm at intervals of time (t) by extracting a 3 mL aliquot from the suspension and separating the solid by centrifugation. Typical spectrophotometric experiments rely on measuring the maximum absorbance, A_{max}; from quantum chemistry, we know that the characteristic absorbance corresponds to an allowed quantized electronic transition. Moreover, classical studies have demonstrated that the absorbance, A_{max}, is directly proportional to the concentration of the probe-molecule in solution as described by the Beer–Lambert law ($A = \varepsilon\, l\, C$), where ε is the absorption coefficient (also called absorptivity, L g^{-1} cm), l is the path length

This journal is © The Royal Society of Chemistry 2019

Catal. Sci. Technol., 2019, 9, 1476–1496 | 1477

of the light through the cell in cm and C is the concentration in g L^{-1}. Therefore, a concentration calibration curve of the probe-molecule in solution can be easily obtained by measuring the A_{max} value of dye solutions with different concentrations. As a first step, a correlation curve was obtained between the concentration of dye in solution (g L^{-1}) and the maximum absorbance value (A_{max}) for each dye measured at their corresponding absorption wavelengths (λ_{max}), i.e. at 554 nm for RhB (λ_{554nm}), 610 nm for IC (λ_{610nm}) and 564 nm for AB (λ_{564nm}).

c) Kinetics

The time evolution of the dye concentration in solution during the experiments was monitored using the equivalence between absorbance and concentration ($A_{max} = C$), however, we measure the absorbance at λ_{max} looking at the whole absorbance spectrum. Concentration data were considered to be reliable as long as the position of each A_{max} peak was not shifted or the shape of the spectrum peak did not change during illumination. The variation of the concentration or relative concentration (C_n/C_0) of a probe-molecule in solution as a function of irradiation time (t) is estimated using eqn (1):

$$\frac{C(t)}{C(t=0)} = \frac{A_{max}(t)}{A_{max}(0)} = \frac{C_n}{C_0} \qquad (1)$$

where C_0 is the initial concentration at $t = 0$, C_n is the concentration at time t during each photocatalytic process, and A_{max} is the experimental absorbance value at the respective time. The decrease of concentration with time, was then related to the rate (r) for each process (adsorption in the dark C_{ads}, photolysis C_{photo}, photodegradation C_{deg}), as expressed in the equations:

$$C_{ads}, C_{photo} = \frac{C_n(t)}{C_0(t_0)} = r_{process} \qquad (1a)$$

$$C_{deg} = \frac{C_n(t)}{C_1(t_1)} = r_{process} \qquad (2)$$

where C_0 is the initial concentration of the probe-molecule in solution measured at t_0 and C_1 is the concentration of the probe-molecule in solution after adsorption–desorption equilibrium measured at dark after a period of time t_1. During adsorption, it is important to maintain a high stirring rate to assure that the reaction is not limited by diffusion of the species and/or depletion of oxygen. The estimation of the apparent reaction rates is described later.

d) Computational calculations of electronic spectra

To understand the different processes that can lead to discoloration of the solution, quantum chemical calculations of the absorbance spectra of the three dyes and their corresponding discoloration/degradation intermediate products were performed. All the electronic calculations were performed with the Gaussian 09 package of programs.[22] Fully optimized structures and harmonic frequencies were obtained at the M05/6-311+G(2d,p) level of theory[23–27] in conjunction with the continuum SMD model using water to mimic a polar environment.[28] Local minima were identified by the absence of imaginary frequencies. The absorption spectra were computed with TD-DFT using the optimized geometries at the same level of theory.[29,30] This TD-DFT investigation was performed in the so-called vertical approximation, i.e. the transition energies toward the lowest excited state were computed considering a frozen geometry (the optimal ground state structure obtained from the optimization). In this approximation, the vibrational degrees of freedom and hence the coupling between nuclear and electronic degrees of freedom (vibronic effects) are neglected. This approach allowed us to determine the nature of different excited states. The accuracy of the relative position of the maximum value and the relative intensities of the peaks depends on the treated case.[31] To achieve accuracy, it would have been necessary to perform TD-DFT in its adiabatic kernel approximation. However, for the purpose of this investigation, TD-DFT vertical approximation is effective because we are not interested in the exact value but rather in whether the shape of the spectrum is comparable with the experimental spectrum.[32]

Results and discussion

The "photocatalytic activity" of a semiconductor is typically quantified by monitoring the variation of the C_n/C_0 value of the dye/molecule in solution (eqn (1)) with irradiation time assuming simple Langmuir–Hinshelwood kinetics,[13] in which an adsorbed monolayer of the probe-molecule is completely in equilibrium. The apparent kinetic rate constant (K_{app}) of the photocatalytic process (discoloration or degradation) is estimated rather than the rate constant (K_{ROS}) of the formation of ROS, which is assumed as a constant[33–36] independently of the dye concentration. However, some authors consider that a first order pseudo steady-state approach must be used for the kinetics equation to fully describe the photocatalysis.[18,37–39] Following this procedure means that the photocatalytic activity is not directly measured but is indirectly estimated from measurements of the absorbance spectra, A_{max}, of the probe-molecule in solution or, in some cases, by measurements of the degradation products (intermediates) or total organic carbon (TOC) content in the solution. Therefore, any photocatalytic experiment using dye molecules should take into account all the possible phenomena that could simultaneously induce a decrease in C_n/C_0 of the dye molecule in solution, such as photolysis (C_{photo}), adsorption (C_{ads}), or the formation of new intermediate products. These intermediates may cause variations in the original absorbance spectrum, A_{max}, which invalidate the use of eqn (1), and this is common during photobleaching or photodegradation (C_{blea}, C_{degra}). In the following, we describe the procedures, and the information obtained from them, to accomplish correct

evaluation of the photocatalytic activity of a semiconductor material using visible light and dyes as the organic pollutants. The processes described are photolysis, adsorption, photocatalytic degradation and mineralization and the results are summarized in Tables 1–3, respectively.

Photolysis

Photolysis refers to the chemical decomposition of molecules by light (photo-decomposition or photochemical reaction), which is defined as catalyzed photolysis according to Serpone.[40] Some chemical compounds are degraded into smaller units by the direct absorption of photons or by reaction with oxidative species generated from the water solution by UV lamps.[41] This is a well-known phenomenon in dyes and pharmaceuticals. The absorption of light by the dye molecule results in photochemically induced homolytic cleavage of the chromophore group, such as the double bond in the indigoid group (NH–C=C–NH)[42] or the C–O=C group in RhB dye.[43] This leads to a loss of color and a decrease in the A_{max}. Therefore, photolysis of the probe-molecule must be evaluated under the defined experimental conditions (λ of lamp, dye concentration, pH, aerated conditions, scavenger substances, etc.), without adding the photocatalyst material. The degree of photo-decomposition [% C_{photo} = (1 − C_{photo}) × 100] of a dye due to light must be known before that dye can be used to evaluate the photocatalytic activity of a material. This effect is critical, especially for high power lamps; however, it is not always reported.[44,45]

In our example, the % C_{photo} values of the three dyes were investigated by irradiating the dye solutions with UV and visible light at the corresponding working dye concentrations and maintaining the solution under magnetic stirring for at least 180 minutes. Each experiment was performed without adding the photocatalytic material, and the profile of C_{photo}(C_n/C_0) was monitored every 30 minutes using eqn (1) through the corresponding A_{max} of each dye. Fig. 1 shows the decrease of C_n/C_0 of all the dyes vs. time during the photoly-

sis evaluation process. The three dyes suffered small decreases in absorbance, suggesting slight decomposition under irradiation, except for RhB, which showed greater stability under visible light. From Table 1, we know that about 10% to 12% of dye was degraded (% C_{photo}) by the action of light; therefore, this 10% to 12% decrease in the absorbance cannot be attributed to photocatalytic action of the photocatalyst because it is due to photolysis.

The next experiment was the evaluation of the fraction of dye adsorbed on the semiconductor surface.

Adsorption

Adsorption of the probe-molecule on the surface of a photocatalyst is a relevant process in photocatalysis that can be estimated by monitoring the concentration ($C_{ads} = C_n/C_0$) of the probe-molecule in solution as a function of immersion time with the specific load of the photocatalytic material in dark and stirred conditions. Adsorption plays an important role in photocatalysis because it is a critical step to achieve the oxidation–reduction of species by the photogenerated electron-hole pairs. Herein, we show that to correctly evaluate the photocatalytic activity of a material, it is essential to measure the fraction of dye molecules adsorbed on its surface once equilibrium is attained, i.e. when a monolayer of adsorbed molecules is formed. For this, we use the following equation:

$$\theta_{ads} = (1 - C_{ads}) \times 100 \qquad (3)$$

The adsorption will influence the effective C_0 of the dye, i.e., the real concentration of the probe-molecule in solution when illumination starts (C_1); therefore, it will influence the estimated photodegradation percentage (% C_{deg} or conversion) and mineralization (% Mine). It should be remembered that adsorption is also a classical method to decrease the concentration of a probe-molecule in solution; this can be tailored depending on the pH of the solution, the catalyst load and the C_0 of the probe-molecule. The θ_{ads} should be measured prior to the irradiation experiments under the experimental conditions (pH, catalyst load, dye concentration, stirring conditions) at which the photocatalytic assays will be performed,[46] but in dark conditions. When dye molecules are
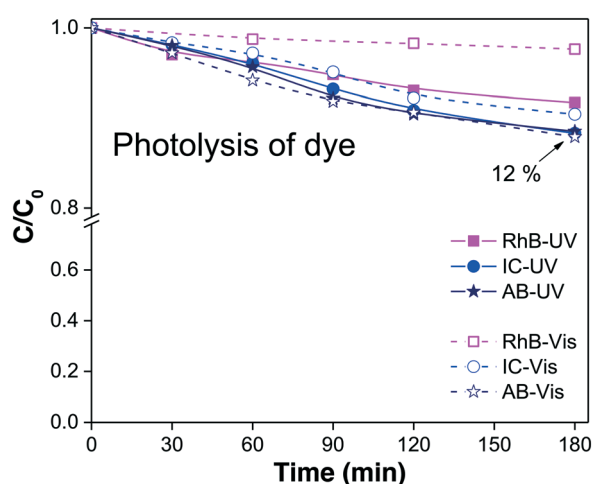

Fig. 1 Variations of the relative concentrations C_{photo} of the three dyes due to the photolysis process when the solution is irradiated with visible light (open symbols) and UV light (filled symbols).

Table 1 Data of the relative concentrations and degrees of photolysis of dye molecules in solution

Dye/irradiation	Dye sol. (ppm)	$C_{photo} = C_n/C_0$	% $C_{photo} = [(1 - C_{photo}) \times 100]$	$Dye_{degraded}$ (ppm)
RhB/UV	5	0.92	8	0.4
RhB/visible	5	0.98	2	0.1
IC/UV	10	0.88	12	1.2
IC/visible	10	0.90	10	1.0
AB/UV	10	0.88	12	1.2
AB/visible	10	0.88	12	1.2

C_0 = initial dye concentration in solution (equal to unity). C_n = dye concentration in solution at 180 min of irradiation. C_{photo} = relative dye concentration after photolysis. % C_{photo} = degree of photolysis of the dye by irradiation.

adsorbed on the surface of a photocatalyst, the maximum absorbance A_{max} of the dye in solution is decreased in comparison to its initial value (C_0). Hence, A_{max} should be measured at periodic time intervals until no more changes are observed in the spectra, indicating that the adsorption–desorption equilibrium has been reached. The decrease in A_{max} is proportional to the fraction of dye molecules adsorbed: θ_{ads}.

To investigate the profiles of C_{ads} of the three different dyes onto α/β-Bi$_2$O$_3$ powders, 15 mL of each dye solution at neutral pH were stirred in the dark. The A_{max} of the dye in solution was acquired every 30 minutes until no further changes were observed. In the case of AB, where a high adsorption was observed at neutral pH, additional experiments were conducted at alkaline pH (9.5) in order to decrease the dye adsorption.

Fig. 2A–C show the absorbance spectra of the three dyes (RhB, IC and AB) at $t = 0$ (continuous line spectra) and after adsorption–desorption equilibrium was reached under the dark-stirred conditions (dashed line spectra). It can be seen that the conditions to apply eqn (1) are fulfilled (no peak shifts); Fig. 2D shows the decreases of C_n/C_0 of all the dyes vs. time, indicating that adsorption–desorption equilibrium was attained after 30 minutes for the three dyes. It is impor-

tant to use the whole spectrum to measure A_{max} or to take care to use proper A_{max} values according to the pH because some dyes (such as methyl orange, which is not included in this investigation) are pH sensitive and their λ_{max} changes with pH.

From Table 2, it is then possible to estimate the maximum θ_{ads} by taking the saturated C_n value at 60 minutes; θ_{ads} changes according to the dye molecule and pH. The adsorption of the dye molecules (and, later, of their degradation products) onto the surface of the photocatalyst is a complex phenomenon that depends strongly on the ionic properties and the pK_a of the molecule, the point of zero charge (PZC) of the photocatalyst, and coulombic and hydrophobic/hydrophilic interactions.

The different percentages of adsorbed molecules observed in these experiments can be readily correlated to the physicochemical properties of the photocatalyst surface and the dyes. For the RhB cationic dye, the θ_{ads} was 0.16 (Table 2), in agreement with our previous report.[21] At pH 6.5, the Bi$_2$O$_3$ surface is partially protonated (H$^+$), because the measured PZC of the α/β-Bi$_2$O$_3$ sample was 6.8.[21] The pK_a of the RhB dye is 3.5; thus, at pH 6.5, the –COOH groups of the cationic RhB$^+$ are deprotonated to –COO$^-$, yielding the zwitterion RhB$^\pm$ (inset

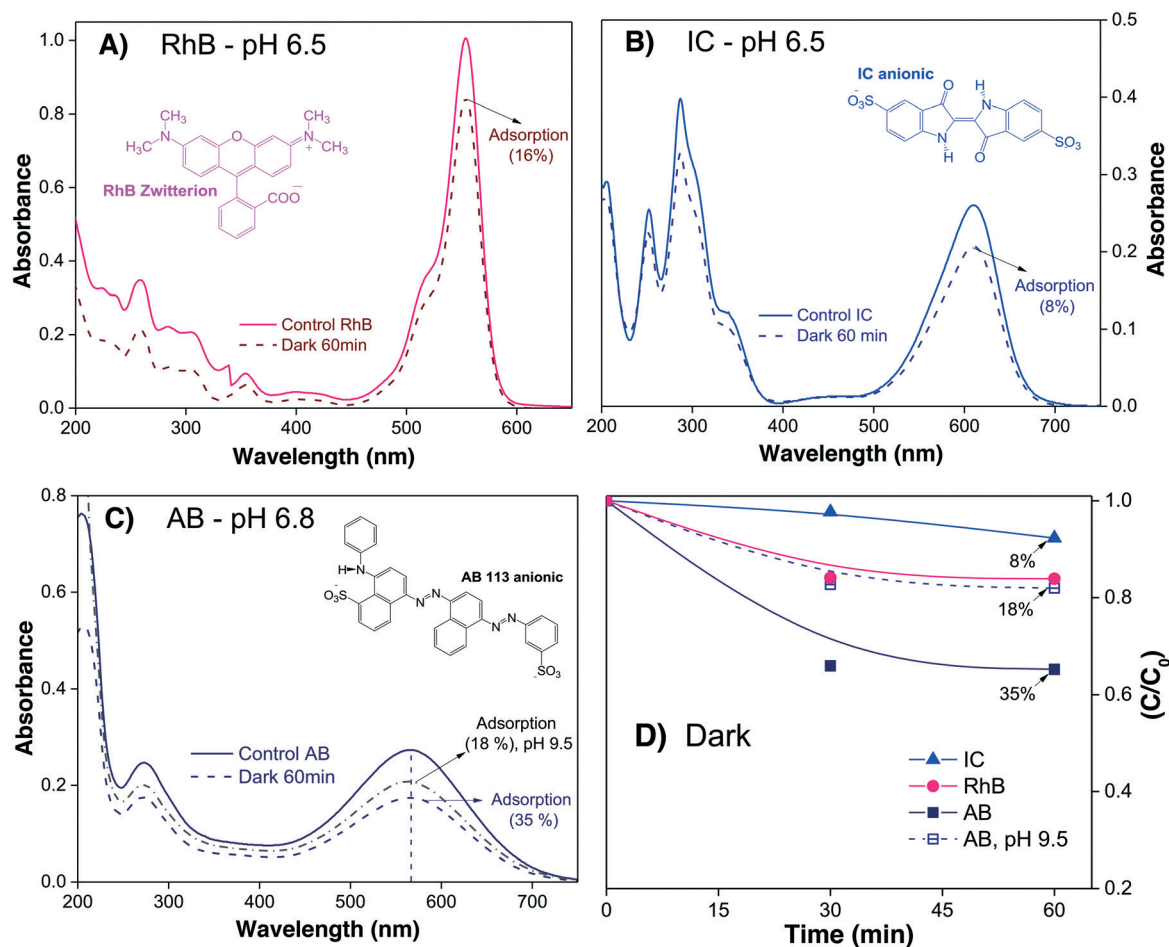**Fig. 2** (A–C) Absorbance spectra of three dye solutions and their evolution after 60 minutes in the dark in the presence of α/β-Bi$_2$O$_3$ powder. D) Variations of C_n/C_0 due to adsorption of the dye molecules on the semiconductor surface in dark conditions; lines are drawn as a visual aid.

Table 2 Data of the relative concentrations and fractions of dyes adsorbed during the adsorption process

| Dye	Dye sol. (ppm)	$C_{ads} = C_n/C_0$	$\theta_{ads} = [(1 - C_{ads})]$	$Dye_{adsorbed}$ (ppm)	C_1 (ppm)
RhB	5	0.84	0.16	0.8	4.2
IC	10	0.92	0.08	0.8	9.2
AB (pH 6.8)	10	0.65	0.35	3.5	6.5
AB (pH 9.5)	10	0.82	0.18	1.8	8.2

C_0 = initial dye concentration in solution (equal to unity). C_n = dye concentration in solution at 60 minutes in dark conditions. C_{ads} = relative concentration of dye in solution after the adsorption process. θ_{ads} = fraction of molecules of the dye adsorbed.

Fig. 2A), which can be adsorbed in the amphoteric sites of Bi_2O_3 through oxygen bonds.[47] For the two anionic dyes, IC and AB, the θ_{ads} values were 0.08 and 0.35, respectively. In both dyes, the anionic behavior is related to the two sulfonated ($-SO_3^-$) groups (inset of Fig. 2B and C), which can be adsorbed onto the photocatalyst surface by forming hydrogen bonds with the protonated surface at pH < 6.8.[48] However, the larger adsorption of the AB dye in comparison to IC suggests a contribution of coulombic interactions. At neutral pH, AB is negatively charged (AB^{2-}) due to its two negatively charged sulfonated groups ($pK_a = 0.5$);[49] thus, it can be electrostatically attracted to the protonated α/β-Bi_2O_3 composite. Similar electrostatic attractions have been reported for azo dyes on TiO_2 and bismuth(III) nitrates.[9,50–52] Thus, the θ_{ads} of the AB dye can be controlled by modifying the solution pH to alkaline, as can be observed in Fig. 2C and D (the dotted line in Fig. 2C refers to pH 9.5). The θ_{ads} of the AB dye

decreased to 0.18 at pH 9.5 because at this pH, the Bi_2O_3 surface is rich in ^-OH species that repel the AB^{2-} species. However, it is also important to consider that in addition to electrostatic interactions, adsorption can occur via hydrophobic–hydrophobic interactions or hydrogen and oxygen bonding. A summary of the different adsorption mechanisms observed for the three dyes on the Bi_2O_3 surface is schematically shown in Fig. 3.

Formally, θ_{ads} should be quantified at different initial dye concentrations to determine the critical value after which no more adsorption is observed; this value will depend on the surface properties of the semiconductor, the probe molecule and the pH value of the solution. However, it is more common to use a fixed initial concentration, even when different semiconductors are compared.

From the above results referring to the same photocatalytic material but different dyes, we can see that the degree of adsorption can be significantly different. Therefore, if the adsorption is not properly considered and eqn (1) is directly used to estimate the photocatalytic degradation achieved after illumination (C_{deg}), i.e., the initial concentration C_0 is used, the degradation will be overestimated. The reason for this overestimation is that the absorbance (A_{max}) is decreased by two different processes, namely adsorption and degradation, while being attributed only to degradation. It was explained earlier that adsorption is necessary for photocatalytic reactions to occur; we cannot assume that all adsorbed molecules are or will be degraded, but it is factual that adsorbed molecules lead to a decrease in the absorbance. Overestimation of photocatalytic degradation due to neglect of the adsorption is a very common error found in the literature;[53–55] this is critical when different materials are
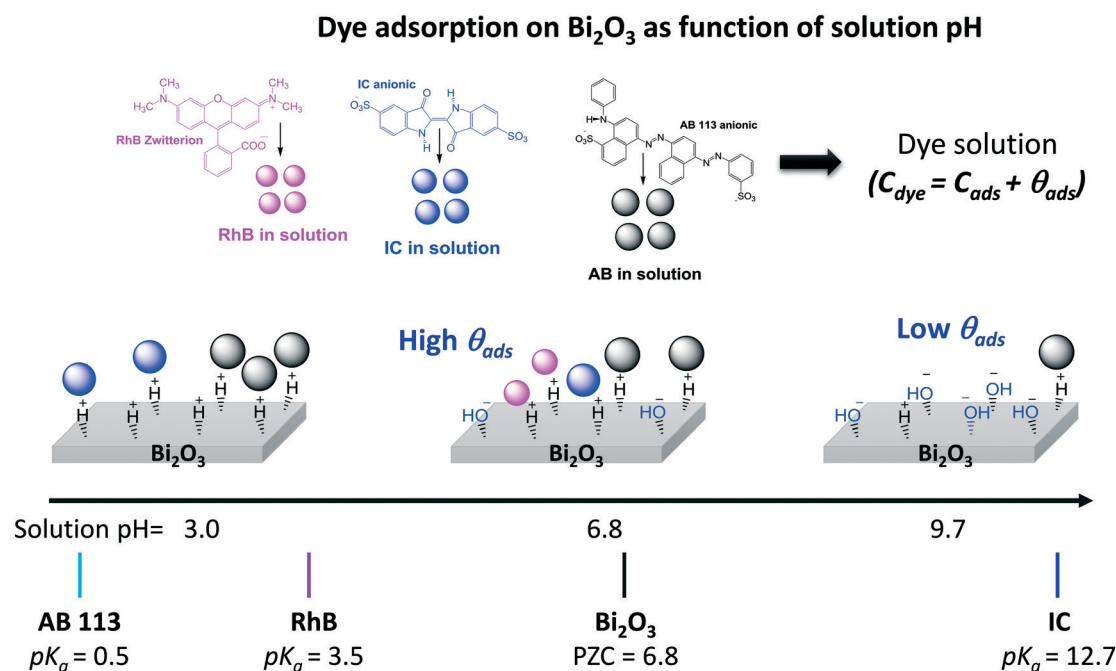
Fig. 3 Schematic of the adsorption processes of the three dyes on Bi_2O_3 at different pH values.

compared and the data are used to select the best photo-catalyst. Moreover, the θ_{ads} will also have an impact on the estimation of the % Mine using any technique based on analysis of the solution because the concentration of total organic carbon (% C_n^{TOC}) in the solution will also decrease.[46]

Once the θ_{ads} is determined, it is possible to evaluate the photocatalytic activity of a photocatalyst knowing the effective concentration of probe-molecules in solution (C_1); proper evaluation should use eqn (2). However, a few competing processes which can occur during the illumination should also be considered.

Competing photocatalytic processes

The evaluation of the "photocatalytic activity" of a photocatalyst material is performed by measuring the color removal (also called discoloration/decoloration) as a function of the irradiation time, preferably under stirring-aerated conditions in order to guarantee that the reaction is not limited by oxygen diffusion. This color removal, % C_{disc}, measured as the decrease in the absorbance A_{max}, is usually interpreted as the photodegradation (% $C_{deg} = (1 - C_{deg}) \times 100$) of the dye molecules due to the action of semiconductor-light interactions. However, there are two competing processes which are not directly due to the photocatalytic activity of the material that can also provoke a decrease in the absorbance A_{max} of the dye in solution under irradiation: *photobleaching* and *sensitization*. These require further explanation prior to the analysis of the photodegradation results.

Photobleaching. A decrease in the intensity of the A_{max} can result from charge transfer (an oxidative or reductive process) between the photo-generated carriers in the photocatalyst and the adsorbed dye molecule, which changes the distribution of the π-conjugated bonds responsible for the visible color and, thus, the absorbance without breaking any chemical bonds (no degradation). Here, we call this discoloration phenomenon *photobleaching*, and we emphasize that it is not a photodegradation process.[56] This phenomenon is common for leuco-dyes that have two molecular arrangements where in one of them, the hydrogenated/reduced form (electron-transfer), is colorless (no absorbance in the visible range). The transformation between the two chemical arrangements can be triggered by different stimuli. Reversible transformations are commonly due to pH or oxidation–reduction reactions, while heat or light lead to irreversible conversions. Some dyes used in the literature, such as crystal violet, indigo carmine, malachite green and rhodamine B, belong to the family of leuco-dyes. For these dyes, the discoloration (observed as a decrease in A_{max}) measured during a photocatalytic experiment can be at least partially due to the *photobleaching* process.[1,3]

We propose that by comparing the whole experimental absorption spectrum and the theoretical spectra of the two leuco-forms of a molecule under study, it is possible to discriminate between *photobleaching* and photodegradation. For some dyes, such as IC, the spectrum of the leuco-form has already been studied;[57,58] therefore, it is known that the formation of the leuco-indigo form can be observed as a strong peak around 390 to 400 nm instead of the peak around 550 to 600 nm of IC. For less well-known dyes, theoretical calculations give us useful information.

Fig. 4A shows the calculated spectra for both IC forms; it can be observed that leuco-IC presents a strong absorption at lower wavelengths, in agreement with experimental observations.[57,58] Thus, during a photocatalytic experiment using IC, the formation of leuco-IC due to the electron transfer process (reduction of IC) can be detected as a shift of the A_{max} to lower wavelengths and/or through the presence of two peaks and two isosbestic points, indicating that the two-chemical species (IC and leuco-IC) are in equilibrium.

Meanwhile, Fig. 4B shows the calculated spectra for RhB$^\pm$ and its corresponding leuco-form, indicating that leuco-RhB does not show a strong absorbance peak in the visible region. Therefore, when using RhB, it is more difficult to discriminate between *photobleaching* and photodegradation processes because the A_{max} situated around 550 nm for RhB$^\pm$ will
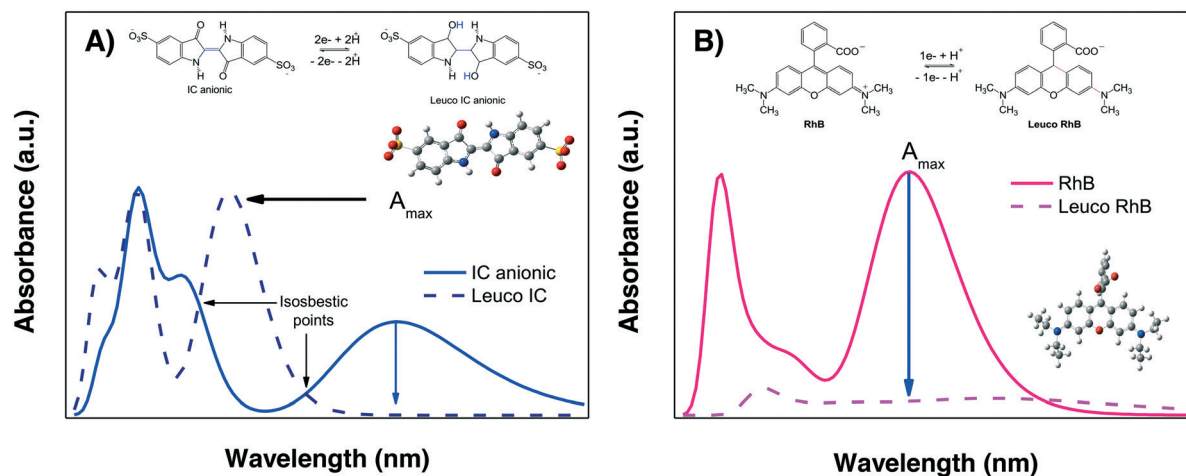

Fig. 4 Calculated absorbance spectra of A) IC and B) RhB and their corresponding leuco forms.

1482 | *Catal. Sci. Technol.*, 2019, **9**, 1476–1496

This journal is © The Royal Society of Chemistry 2019

decrease without other spectral changes that can indicate the formation of leuco-RhB. Although Ma *et al.*[43] suggested that leuco-RhB presents a slightly yellow color with a weak absorbance peak at 420 nm, this was not confirmed by calculations or a literature review.

It is important to mention that the formation of the leuco forms, *i.e.* leuco-IC[58,59] and leuco-RhB dyes,[43] typically occurs under conditions where the oxygen diffusion rate is limited, such as in N_2 atmosphere, low stirring conditions or in the presence of hydrogenating/reducing agents ($NaHB_4$, NH_2NH_2), also called sacrificial electron donors.

In the present work, the photocatalytic degradation of the three dyes was performed at a high stirring rate, *i.e.* 1200 rpm, generating oxidizing conditions where leuco forms are not favored. The absorption spectra of the RhB and the IC dye solutions after irradiation (both UV and visible) in the presence of the test α/β-Bi_2O_3 semiconductor are shown in Fig. 5 and 6, respectively. The figures show that on the one hand, similarities exist between the experimental and calculated spectra of both dyes. On the other hand, for the IC dye (Fig. 6), there is no signal for either the leuco-IC absorption or isosbestic points, indicating that the *photobleaching* process of the dianionic IC^{2-} dye is not relevant to our experiments.

For RhB, nothing certain can be stated because only a decrease in the maximum (A_{max}) is observed; this decrease could be due to either photodegradation or photobleaching. Thus, the above analysis suggests that the use of RhB as a probe-molecule to evaluate the photocatalytic activity of a material is dubious, even though it has been widely employed.[60–65]

The other mechanism that can lead to a decrease in the C_n/C_1 ratio but does not reflect the catalytic activity of the photocatalyst is *sensitization*; it is usually associated with dyes but can occur in any organic molecule with absorption bands in the UV or visible region of the spectrum, as long as the incident light is resonant with the absorption.

Sensitization. During sensitization, the organic probe-molecule (S) itself functions as a photosensitizer, resonantly absorbing the incident light (S^*) and transferring electrons to the conduction band of the photocatalyst; this results in the formation of an unstable cation radical ($S^{+\bullet}$) which is easily degraded, as has been reported previously.[3,66,67] This is a synergistic process that involves the photocatalyst, the adsorbed dye molecule and the resonant absorption of light; it can only occur when the wavelength of the incident light can be absorbed by the organic probe-molecule.[68] In the case of
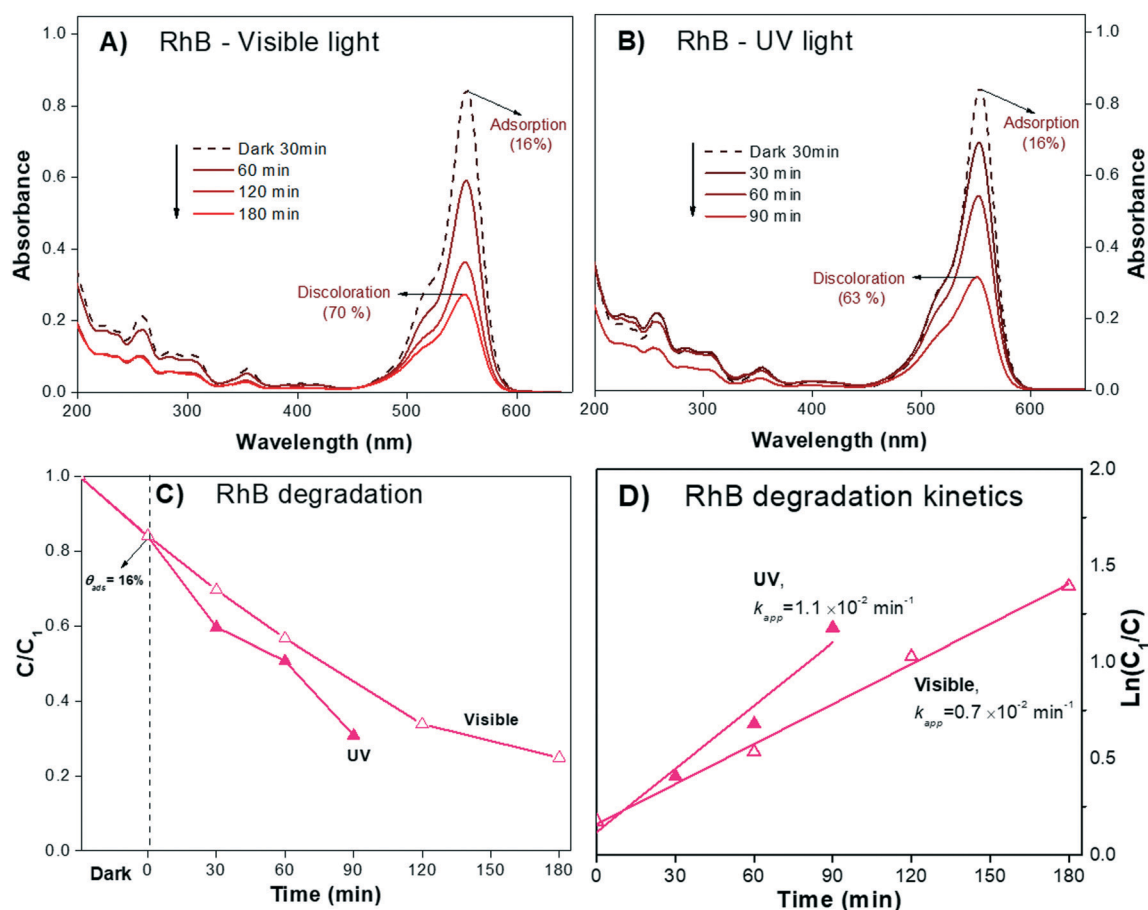

Fig. 5 Absorbance spectra of zwitterion RhB solution during photodegradation under (A) visible light and (B) UV light. C) Relative concentrations of dye with and without correction due to the change in the initial concentration by adsorption and D) linear fits of the $\ln(C_0/C)$ plots of the degradation under visible and UV light to obtain the apparent reaction rate.
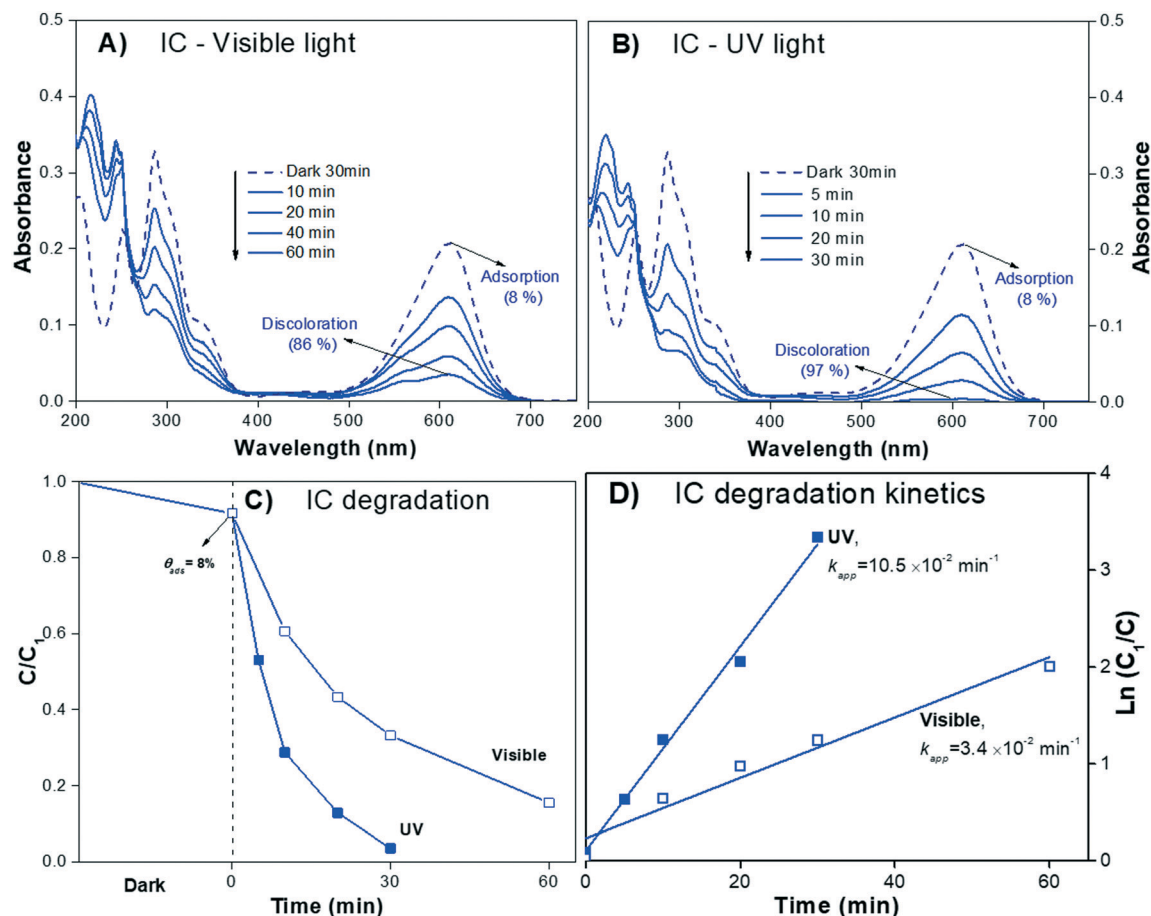
Fig. 6 Absorbance spectra of the IC solution during photodegradation under (A) visible light and (B) UV light. C) Relative concentrations of dye with and without correction due to the change in the initial concentration by adsorption and D) linear fits of the $\ln(C_0/C)$ plots of the degradation under visible and UV light to obtain the apparent reaction rate.

dyes, these wavelengths are in the visible range of the spectrum. This process can actually lead to the formation of intermediate molecules; this has been observed for RhB, which is transformed *via* an efficient *N*-deethylation sensitization mechanism under visible light in the presence of different photocatalysts.[3,60,65,69,70] In these cases, a hypsochromic shift of the A_{max} of RhB from 554 nm to lower wavelengths (λ) is detected. Sensitization is not a negative effect; however, if sensitization occurs, then one cannot reach a conclusion about the efficiency of a semiconductor material as a visible-light photocatalyst.

One proposed method to detect sensitization is based on the measurement of an action spectrum, as suggested by Lee *et al.*[71] The action spectrum is a plot of the photonic efficiency *versus* the wavelength; this is not easily obtained for all materials, but it enables clear discrimination between sensitization and photocatalytic activity.[72] When the action spectra cannot be measured, an indirect method to recognize if the sensitization process has occurred is to compare the degrees of photodiscoloration obtained using visible light and using another wavelength range which is not resonant with the absorbance spectrum of the dye, such as UV. If the visible-light reaction rate (r) is greater than or similar to that

obtained using UV light, sensitization may be playing an important role in the final response.[3,73]

In order to determine the possible contribution of the sensitization process for the Bi_2O_3 material, photodiscoloration experiments were performed using both UV and visible light. The solution volumes and photocatalyst loads were the same as previously mentioned. The A_{max} values of the dyes are centered at λ_{554nm} (RhB), λ_{610nm} (IC) and λ_{565nm} (AB), and the white lamp used emits in the whole range between 420 and 640 nm. Therefore, it is possible to excite all three dye molecules by resonant absorption.

The sensitization process was tested for the three dyes by analyzing the whole absorbance spectrum of the dye solution and comparing the time to achieve similar decrements in the A_{max} value under UV and visible light.

The absorbance spectra of the zwitterion $RhB^{\pm}$ dye solution (pH 6.5) during the irradiation process under visible and UV light are presented in Fig. 5A and B, respectively. The $RhB^{\pm}$ in solution exhibited a characteristic A_{max} at λ_{554nm} that slowly decreased over 180 min of visible irradiation. Under UV light irradiation (350 to 400 nm, Fig. 5B), the spectrum attained a similar decrease in A_{max} in only 90 minutes. For both irradiations, no shifts of A_{max} were observed, suggesting

negligible contribution of the *N*-deethylation sensitization process described earlier; this was also expected from the quantum chemical calculations, as shown later.

The absorbance spectra of the IC dye solution (pH 6.5) during the irradiation process (visible and UV light) are presented in Fig. 6A and B, respectively. The IC solution exhibited the characteristic A_{max} at λ_{610nm}, which decreased almost to zero over 30 min under UV irradiation; meanwhile, under visible light, the A_{max} of IC decreased but did not reach zero after 60 min of irradiation, suggesting that the sensitization process when using IC dye is negligible.

The evaluation of the anionic AB dye was performed at pH 9.5 to avoid the strong adsorption observed at neutral pH. The absorbance spectra of the AB dye during visible and UV irradiation are shown in Fig. 7A and B, respectively; it can be observed that the decreases in A_{max} are very similar for both lights, attaining similar values after 90 min. This effect can be taken as an indication that sensitization is playing an important role.

Finally, after estimating the contributions of different processes (photolysis (% C_{photo}), adsorption (θ_{ads}), photobleaching and sensitization) to the variation in the absorbance A_{max} of the dye solution, it is possible to proceed with evaluation of the photodegradation (% C_{deg}) of the dye molecule.

Photodegradation

Photodegradation, also called photoconversion, is the molecular cleavage of a probe molecule into diverse intermediate products; it can be initiated by oxidative processes through the interaction of adsorbed dye molecules with either the photogenerated holes or the reactive oxygen species (superoxide or hydroxyl radicals) generated on the surface of the photocatalyst by the photocarriers.

As described previously, the evolution of the dye concentration ($C_{deg} = C_n/C_1$) with respect to the irradiation time can be estimated from the variations in the A_{max}, assuming the same approach ($A_{max} = C$). However, when the dye molecule

is degraded into secondary or intermediate products that have different ε values but absorb at similar λ_{max} values to the original dye, the straightforward correlation between A_{max} and the concentration of the dye in solution (see eqn (1)) is no longer valid.[20,74] This is usually the first source of error for the estimation of the photodegradation activity (% C_{deg}) of a photocatalyst. Therefore, we propose that instead of reporting only the C_n/C_1 ratio, a careful analysis of the spectral changes in the whole energy range should be presented. By analyzing the whole spectra, it is possible to detect the presence of intermediates or degradation products, which indicate that photodegradation of the probe-molecule is actually occurring; moreover, depending on the spectral changes, the validity of eqn (1) can be determined. The expected modifications in the whole absorbance spectrum include a) broadening of the main A_{max} due to intermediates that absorb close to the characteristic absorbance (λ_{max}) of the selected molecule, but with different absorptivities; b) appearance of new absorbance peaks (A_{max}^*) related to intermediates with characteristic λ_{max}^* values well below those of the original probe-molecule, so that they do not overlap; and c) the presence of isosbestic points, which can indicate the presence of two or more molecules in equilibrium. Ideally, one could experimentally determine the contribution of the intermediates to the spectral changes. However, this requires the lengthy procedure of obtaining pure substances of all the intermediates and drawing calibration curves to compare their absorptivities to that of the test molecule.

One feasible approach, which we propose in this paper, is the use of quantum chemical calculations to obtain prior knowledge about the processes expected during the degradation of a particular organic molecule.

Once the qualitative photodegradation and the validity of eqn (1) are confirmed, the percentage of degradation (% C_{deg} = 1 − C_{deg} × 100) or the profile C_n/C_1 are estimated to evaluate the kinetic parameters. From the analysis, the apparent kinetic rate constant (K_{app}) can be used to compare the activity of the photocatalyst to that of other materials. However, in
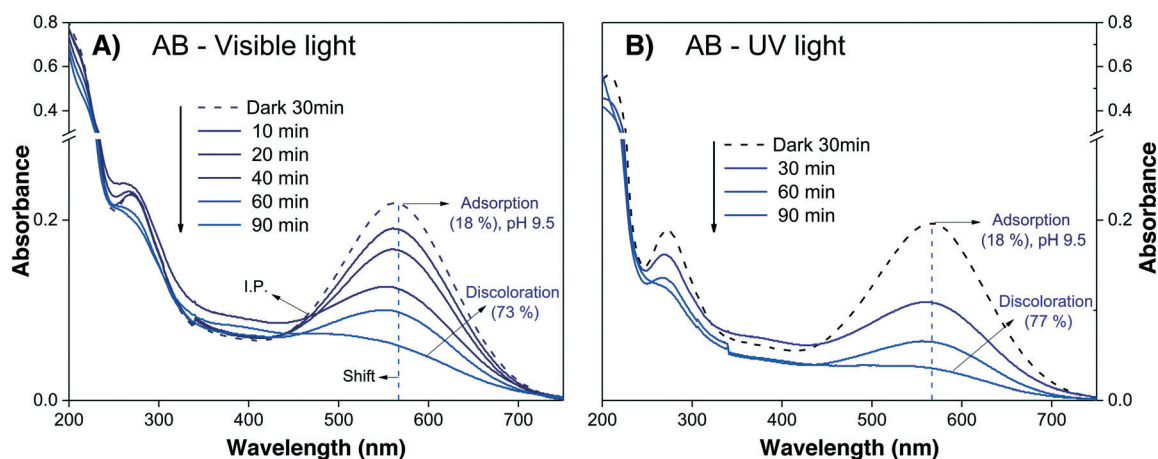

Fig. 7 Absorbance spectra of the AB solution at pH 9.5 during photodegradation under (A) visible light and (B) UV light.

general, the validity of eqn (1) is assumed but not demonstrated because the whole spectra are not analyzed. Before proceeding with the analysis for each of the dyes, we will first review the estimation of the kinetic parameters.

Kinetic parameters. For unimolecular surface reactions, the conversion rate (r) or the rate constant (k_r) of the formation of intermediate products is usually described according to the law of mass-action; the rate is given by:

$$r = -\frac{dC_1(t)}{d(t)} = k_r \theta_{ads} \tag{4}$$

where $C_1(t)$ is the dye concentration in solution at time t after dark absorption, k_r is the reaction rate constant, and (θ_{ads}) is the fraction of probe-molecules adsorbed on the photocatalyst surface. The negative sign indicates that the dye concentration decreases. It is commonly assumed that the adsorption–desorption (θ_{ads}) equilibrium follows a Langmuir adsorption isotherm;[17,18,37] therefore, (k_r) is estimated assuming that during the photocatalytic reactions, the (θ_{ads}) equilibrium is still satisfied, given by

$$\theta_{ads} = \frac{K_s C_1}{1 + K_s C_1} \tag{5}$$

where K_s is the specific adsorption rate constant of the probe-molecule. However, as the reaction progresses, the dye molecules and the formed intermediate products (I_i) contend for adsorption on the surface (θ_{ads}); therefore, assuming the L–H kinetic model, the reaction rate during the photoreaction takes the form:

$$r = k_r \theta_{ads} = \frac{k_r K_s C_1}{1 + K_s C_1 + \sum_{i=1}^{n} K_{si} I_i} \tag{6}$$

where K_{si} is the adsorption coefficient of the intermediate products. Because it is not possible to estimate K_{si}, it is commonly assumed to be equal to the adsorption coefficient of the probe-molecule.[33]

This type of unimolecular surface reaction shows two limiting rate laws, corresponding to the two extreme behaviors of the Langmuir isotherm:

a) At high initial dye concentrations: For C_1 values that lead to steady state surface coverage close to unity ($\theta_{ads} \approx 1$), a zeroth order reaction is observed ($r = k_r$). This means that the surface reaction rate depends neither on the dye concentration nor on the concentration of intermediate products in solution.

b) At low initial dye concentrations: For C_1 values not high enough to saturate the adsorption sites, the steady state surface coverage is much smaller than unity ($\theta_{ads} \ll 1$); thus, a first order reaction is obtained. This means that the surface reaction rate depends on the initial dye concentration and on the concentration of intermediate products in the solution.

In this case, eqn (5) can be approximated as

$$r = k_r \theta_{ads} \approx k_r K_s C_1(t) = K_{app} C_1(t) \tag{7}$$

which defines the commonly used kinetic parameter K_{app}. Integration of eqn (7) leads to a simple method to estimate K_{app} as the slope of the plot:

$$-\ln \frac{C_n}{C_1} = K_{app} t \tag{8}$$

Therefore, by plotting the $-\ln(C_n/C_1)$ data obtained from the analysis of the spectra using eqn (1) *versus* the irradiation time, t, K_{app} can be estimated if a good linear correlation is observed.

Despite the critical revisions made by many authors[18,38,75,76] regarding the use of the Langmuir–Hinshelwood (L–H) approximation to describe the influence of the initial dye concentration (C_1) on the reaction rate (k_r), this approach is currently a "standard method" to compare the activities of different photocatalysts. It is beyond our objectives to analyze this controversy more deeply; however, the L–H is certainly a rough approximation which should be taken carefully. There is also the controversial point of choosing the zeroth or first order approximation. The common practice is that when there is a deviation from the first-order approximation, the logarithmic "C_n/C_1 vs. t" plot does not show a linear trend, and the authors must choose a decreased number of experimental points to fit the linear logarithmic plot. However, this can lead to significant errors in the K_{app} values but also to a wrong interpretation of the results. In a recent paper, Asenjo et al.[37] suggested performing direct fitting of the "$C_n(t)$ vs. t" plot using non-linear minimization algorithms instead of arbitrarily assuming the order of the reaction.

In the following, we will examine the photodegradation of the three dyes, and when the conditions mentioned above are fulfilled, the % C_{deg} and K_{app} values will be estimated.

Photodegradation of RhB. The calculated spectra of the zwitterion RhB$^{\pm}$, the corresponding N-deethylated products and the spectra of the photodegradation intermediates of RhB are shown in Fig. 8A and B, respectively. As discussed above, it has been shown that during sensitization,[70,77,78] RhB is degraded through the formation of N-deethylation intermediates, which exhibit A_{max} values at lower wavelengths (λ_{495nm}) than the A_{max} of RhB$^{\pm}$ (λ_{554nm}). The calculated spectra of these N-deethylation intermediates are shown in Fig. 8A (RhB-1 to RhB-4), showing that the maximum A_{max} is shifted to lower wavelengths ($\lambda_{554 \rightarrow 495nm}$) and there are small differences in the peak intensity of these intermediates. Therefore, experimentally, during the sensitization, a shift in the absorbance spectrum of the dye solution to lower wavelengths is expected as the N-deethylation intermediates are formed. An isosbestic point can be observed when two chemical species are in equilibrium; however, if more intermediate products are formed, the isosbestic point will be blurred. The N-deethylation intermediates represent the molecular degradation of RhB$^{\pm}$ induced by sensitization, which can be used as a method to augment the photocatalytic activity of wide

1486 | *Catal. Sci. Technol.*, 2019, **9**, 1476–1496

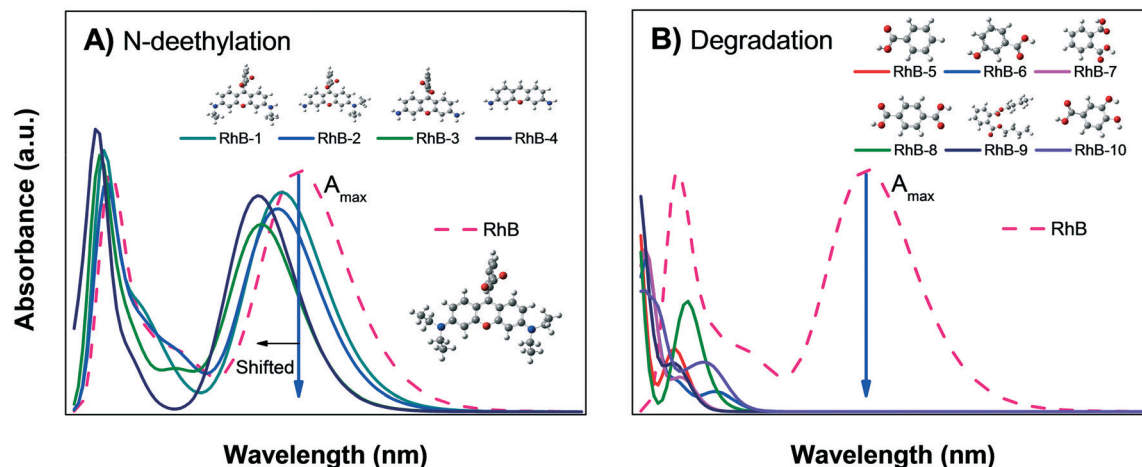This journal is © The Royal Society of Chemistry 2019

Fig. 8 Calculated absorbance spectra of zwitterionic RhB; A) *N*-deethylation sensitization and B) degradation into small organic molecules.

band gap semiconductors, such as TiO_2 and ZnO,[79] and extend their activity towards the visible light range. However, the estimation of the profile of degradation (C_n/C_1 plot) using eqn (1) is not correct because the absorptivity (ε) of $RhB^{\pm}$ is different from that of the degradation products. However, even when *N*-deethylation is detected, it is common for authors to calculate the C_n/C_1 ratio using eqn (1) and mistakenly assume that the decrease is due to the photocatalytic activity of the material.[80,81]

Fig. 8B shows the calculated absorbance spectra for the main degradation products (RhB-5 to RhB-10) of $RhB^{\pm}$ that might be formed during photodegradation; this shows that the degradation products have no absorbance peaks in the visible region. Therefore, when photodegradation occurs, the A_{max} of the $RhB^{\pm}$ solution will decrease without showing spectral changes except for a possible increment in the absorption at very low wavelengths UV region.

Comparison of the experimental data shown in Fig. 5A and B with Fig. 8A and B suggest that the decrease in the A_{max} of zwitterion $RhB^{\pm}$ dye solution as a function of irradiation time is due to photodegradation of the molecule; since no evidence of the *N*-deethylation process was observed. However, a similar decrease in A_{max} could also be due to the photobleaching of RhB, as explained in Fig. 4B. Hence, the only method to distinguish between these two processes (photodegradation and photobleaching of RhB) is to leave

the solution in the dark for a certain time (overnight) and see if the RhB color returns; this is because photobleaching is reversible, while degradation is not.

After doing this, we can be certain that eqn (1) is valid, and it is possible to estimate the photodegradation rate (% C_{deg}) by monitoring the decrease in C_n/C_1 as a function of time, as shown in Fig. 5C.

Using the C_n/C_1 data (Fig. 5C), K_{app} (Table 3) was estimated from the linear fit of eqn (8). The results show that K_{app} is two times larger under UV (1.1×10^{-2} min^{-1}) light illumination than under visible light (0.7×10^{-2} min^{-1}), supporting that sensitization and *N*-deethylation indeed did not take place for RhB.

The previous analysis confirmed that the color removal observed in Fig. 5A and B for RhB can be attributed to photodegradation of the dye molecules through the formation of intermediate products (Fig. 8B) and due to the catalytic activity of the α/β-Bi_2O_3 composite.

Photodegradation of IC. IC dye was chosen because it is well known that its photodegradation pathway leads to the formation of intermediate products that can be monitored by measuring the spectral region between 210 and 260 nm.[21,82–84] In environments rich in oxygen, the indigoid group (NHC═CNH) of the IC structure breaks *via* an oxidative process into isatin sulfonic or 2-amino-5-sulfobenzoic acid, both of which exhibit absorbance in the UV spectral

Table 3 Data of the relative concentrations of dyes during the photodegradation process

Dye/irradiation	C_1 (ppm)	% C_1^{TOC}	$C_{deg} = C_n/C_1$	% $C_{deg} = [(1 - C_{deg}) \times 100]$	K_{app} (×10^{-2} min^{-1})	Dye$_{deg}$ (ppm)
RhB/UV	4.2	84	0.30	70	1.1	2.9
RhB/visible			0.37	63	0.7	2.6
IC/UV	9.2	92	0.03 (30 min)	97	10.5	8.9
IC/visible			0.12 (60 min)	86	3.4	7.9
AB/UV	8.2	82	0.27	Invalid	Invalid	5.9
AB/visible			0.23	Invalid	Invalid	6.3

C_1 = effective dye concentration. % C_1^{TOC} = total organic carbon of effective dye solution calculated from C_1. For AB, the photodegradation reaction was carried out at pH 9.5. C_{deg} = relative concentration of dye in solution measured at 90 min of irradiation.

This journal is © The Royal Society of Chemistry 2019

Catal. Sci. Technol., 2019, **9**, 1476–1496 | **1487**

region.[82–84] This was also confirmed by the quantum chemical calculations of the spectra of the dianion IC^{2-} and its corresponding intermediate products, as shown in Fig. 9.

None of the degradation products showed absorbance peaks that overlap the absorbance of the IC solution in the visible region; therefore, during photodegradation, the A_{max} of the IC dye should continuously decrease proportionally to the concentration. Thus, C_n/C_1 can be properly estimated from the decrease of the A_{max}, and the photodegradation rate (% C_{deg}) can be correctly determined. Moreover, when analyzing the whole calculated absorbance spectra, two interesting features are expected: a) the intensity of the low wavelength ($\lambda < 285$ nm) peaks might initially increase, but eventually, for a complete degradation, they should decrease following the main absorbance peak, and b) isosbestic points might be observed when the degradation products are in equilibrium with the IC dye in solution. These isosbestic points are expected to appear at lower wavelengths than that of the leuco form (see Fig. 4A); therefore, for IC dye, analysis of the isosbestic points allows us to differentiate between degradation and photobleaching processes.

The evolution of the spectra during the irradiation of the IC solution shown in Fig. 6A and B clearly demonstrates the photodegradation (% C_{deg}) of the dye. Both signals due to IC (λ_{285nm} and λ_{610nm}) decrease with irradiation time, while the two UV peaks at λ_{219nm} and λ_{245nm} increase in intensity. These absorbace peaks due to the degradation products have been observed by other authors[84,85] and the theoretical spectra are shown in Fig. 9; meanwhile, the corresponding isosbestic point is observed around λ_{251nm}. The changes in all the spectral peaks are associated with the destruction of the indigoid group (NHC=CNH) of the IC dye structure due to the photodegradation process, with the subsequent formation of the typical intermediate products. Moreover, from the spectral analysis, it is possible to conclude that the photodegradation process of the secondary products was not complete under UV light (up to 30 min) or under visible light (up to 60 min) irradiation because both UV peaks and the isosbestic point persist.
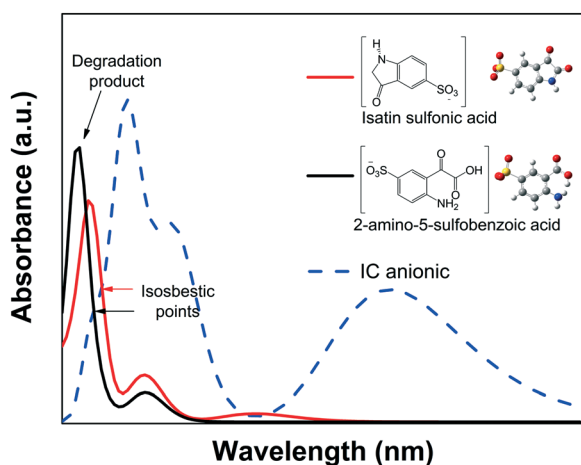
However, the evidence of the degradation of the IC chromophore group allows us to correctly estimate the decrease in the C_n/C_1 value (Fig. 6C). Note that the correction due to the adsorption is less significant than for RhB. Fig. 6D shows the photodegradation kinetic plot, where the K_{app} can be readily determined. It can be seen from Table 3 that K_{app} is lower under visible light (3.4×10^{-2} min^{-1}) than under UV light (10.5×10^{-2} min^{-1}), confirming the negligible impact of the sensitization process.

Photodegradation of AB. Analysis of the photodegradation of the AB dye solution was more challenging due to the presence of a large number of degradation products. The calculated spectra of the dianion AB dye and its corresponding degradation products are shown in Fig. 10A and B. The spectra of some of the products exhibit absorbance peaks at lower wavelengths (Fig. 10A), while others (AB-1, AB-3 and AB-7) partially overlap the A_{max} of AB (Fig. 10B). Therefore, the degradation pathway of AB dye can lead simultaneously to both blue-shifting and broadening of the absorbance spectra. Moreover, due to the different absorptivity values of the AB-1, AB-3 and AB-7 products, the correlation between A_{max} of the AB^{2-} dye and the concentration is no longer valid. Therefore, neither the % C_{deg} of AB dye nor the apparent kinetic rate constant (K_{app}) can be reliably determined.

The results of the AB degradation shown in Fig. 7A and B also reflect the complexity of this dye in terms of its degradation pathway. First, the anionic AB dye is highly adsorbed onto the photocatalyst surface, and the color removal rate is similar under both lights; this suggests a contribution of the sensitization process. Second, the UV-light induced spectral evolution is different from the visible-light induced spectral evolution, suggesting that the intermediates arising from the destruction of the AB dye structure are peculiar to the illumination type. During visible illumination, it is possible to observe a shift in the A_{max} of the AB solution from λ_{565nm} to λ_{550nm}, and there is an isosbestic point at λ_{460nm} after 40 min; this suggests the presence of two chemical species in equilibrium. Finally, after 90 min of irradiation, the spectrum displayed an increase in the absorbance around λ_{450nm}, indicating the formation of another intermediate product. Meanwhile, under UV light irradiation (Fig. 7B), a continuous decrease in A_{max} is observed, without peak shifts or isosbestic points. However, the expected interferences deduced from the theoretical calculations indicate that the correlation between A_{max} and C_n of the AB dye is not valid; consequently, the % C_{deg} value of the AB dye cannot be determined (Table 3). This suggests that AB dye is not a good probe molecule.

Mineralization

The degradation of the original organic probe-molecule to CO_2 and H_2O is the final goal of the photocatalytic process of organic pollutants, where the total organic carbon content (% C_n^{TOC}) at a given irradiation time is reduced to zero.[1,3,4] The organic probe-molecule breaks down into intermediate

Fig. 9 Calculated absorbance spectra of IC and its two intermediate products.

1488 | *Catal. Sci. Technol.*, 2019, **9**, 1476–1496

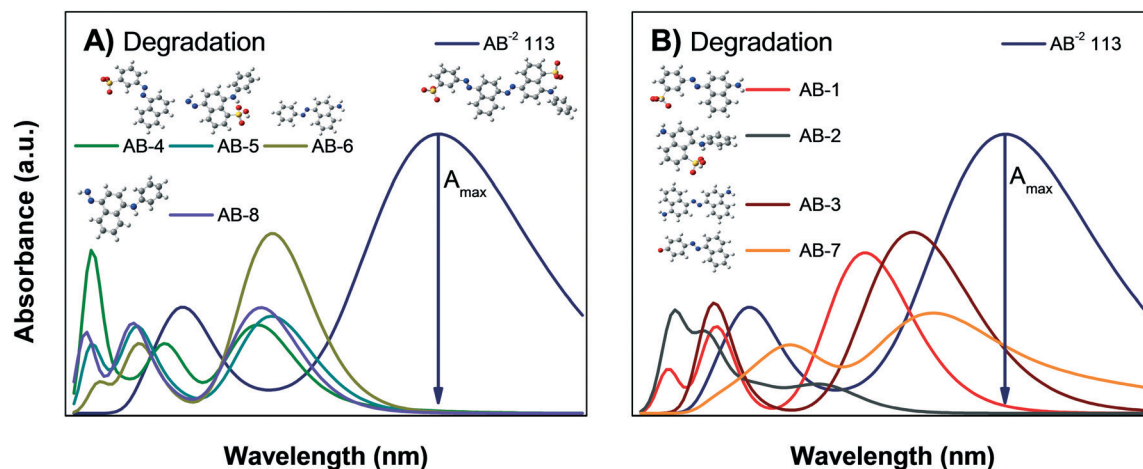This journal is © The Royal Society of Chemistry 2019

Fig. 10 Calculated absorbance spectra of AB and multiple intermediates of the degradation process: A) intermediates that do not interfere with the AB absorbance and B) intermediates AB-1, AB-3 and AB-7, which clearly interfere with the A_{max} value.

products, which are finally mineralized through the oxidative attack of powerful oxidizing species, *i.e.* the hydroxyl radical, or by direct attack of the photogenerated holes.[75,86] As described before, it is not possible to evaluate mineralization using spectrophotometric techniques. However, if no spectral changes are observed even during long periods of irradiation, % C_n^{TOC} will be unaltered, and the photodegradation and mineralization will certainly be negligible. If spectral changes occur that are not associated to adsorption, such as a decrease in A_{max}, a shift of the absorbance peak (usually to lower wavelengths) or the appearance of new absorbance peaks (also at lower wavelengths), it is worthwhile to perform a total organic carbon (TOC) content analysis. To perform this analysis, it is very important to determine the effective carbon content available for mineralization:

$$\% \ C_1^{TOC} = \% \ C_0^{TOC} - \% \ \theta_{ads}^{TOC} \qquad (9)$$

i.e. we must also consider the fraction of organic molecules that were initially adsorbed on the photocatalyst surface (θ_{ads}). The formation of leuco-form dye molecules or diverse intermediates (I_i) will contribute roughly the same amount of carbon as the initial organic pollutants; therefore, there is no need for corrections due to photolysis or photobleaching.

The percentage of mineralization at a given time is then calculated from the effective carbon content as follows:

$$\% \ \text{Mine} = \% \ C_1^{TOC} - \% \ C_n^{TOC} \qquad (10)$$

As observed by these definitions, the fraction of adsorbed molecules must be properly considered to avoid false values for both the photodegradation (% C_{deg})[53] and mineralization (% Mine) results.

Following the case study, the mineralization induced by the α/β-Bi$_2$O$_3$ material was evaluated in a complementary experiment by comparing the effective or initial total organic

carbon (% C_1^{TOC}) of the dye solution with the TOC values after irradiation for extended periods of time (% C_n^{TOC}). The dye concentration, photocatalyst load and light illumination conditions were the same as described above; the pH was nearly neutral for the RhB and IC dyes and basic (9.5) for the AB dye in order to limit the adsorption. The TOC analysis was carried out using a Shimadzu TOC-L analyzer with a high sensibility column.

Fig. 11 shows the decrease of the % C_n^{TOC} values achieved by the α/β-Bi$_2$O$_3$ photocatalyst for the three dye solutions at different visible light exposure times. The percentages of photodegradation (% C_{deg}) measured by the spectrophotometric technique are also included in Fig. 11. The figure shows that during the first 60 min of irradiation, the decrement of % C_n^{TOC} is comparable to the adsorption percentage
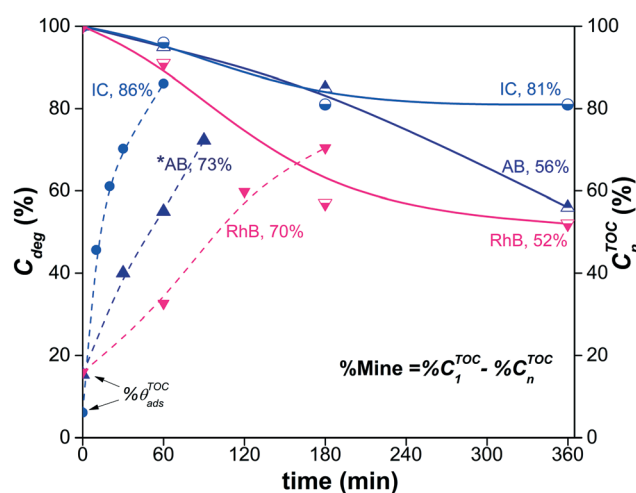

Fig. 11 Percentage of visible-light photodegradation or conversion of the IC and RhB dyes, where a good estimation of the C/C_0 data could be obtained, and the TOC decrease percentages of the three dye solutions at longer irradiation times under visible light. For the AB dye at alkaline pH, saturation of % C_n^{TOC} was not observed up to 360 min.

measured by the spectrophotometric technique, suggesting that the decreased carbon content in solution is mainly due to the adsorption (% θ_{ads}^{TOC}). At longer irradiation times (360 min), % C_n^{TOC} values of 52%, 81% and 56% were achieved for RhB, IC and AB, respectively. However, using eqn (9) and (10), the % Mine values actually achieved (Fig. 12) are 32%, 11% and 26% for RhB, IC and AB, respectively. These values are lower than those obtained for the % C_{deg}; this suggests that during the spectrophotometric experiments, we observed photodiscoloration of the dye, but the intermediate products (% I_i^{TOC}) remained in the solution without being degraded. Therefore, this confirms that the estimated % C_{deg} does not necessarily reflect the mineralization of the probe-molecule.

Fig. 11 also shows that for the RhB and IC dyes, saturation of the % C_n^{TOC} occurred at 180 min; this is unexpected because the formation of reactive oxygen species and holes, which are responsible for the mineralization, is typically linear during the irradiation time.[87–89] This saturation is an indication that the % C_n^{TOC} value obtained at 180 min is probably due to a decrease of the TOC contribution from the intermediate products (% I_i^{TOC}) in solution due to their adsorption on the surface of the semiconductor. The spectrophotometric technique provides us with information about the adsorption of the dye molecules but not about the adsorption of the intermediates. Similar results were reported in ref. 90 for the IC dye, in which complete mineralization was not achieved using α-Bi$_2$O$_3$.

The corrected values for % Mine using the effective initial TOC values after adsorption are presented in Fig. 12, including a summary of the data obtained during the different steps. The low % Mine suggests that the intermediates created during the irradiation by sensitization and/or photodegradation remain in the solution.

The message is that TOC analysis, similar to the spectrophotometric technique, also requires correction due to adsorption in order to provide reliable information about the photocatalytic activity of semiconductors.

Discussion

The aim of this paper is to show that by combining theoretical and experimental data, it is possible to distinguish and properly quantify the different processes occurring during the evaluation of the photocatalytic activity of semiconductors using dye solutions, which is of significant importance to reach adequate conclusions. Three dyes were employed to this purpose. For each dye, spectrophotometric

Competing photocatalytic processes during the photodiscoloration of dye using Bi$_2$O$_3$

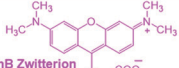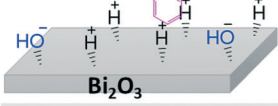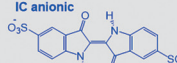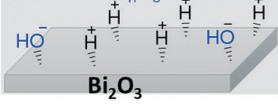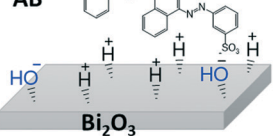| Dye	Adsorption θ_{ads}	Photolysis (%C_{photo})	Sensitization	Photobleaching	Degradation (%C_{deg})		TOC Analysis (%C_n^{TOC})	Mineraliz. (%Mine)
					Vis.	UV		
RhB (RhB Zwitterion)	16	2	No	No	70	63	52	32
IC (IC anionic)	8	10	No	No	86 (60 min)	97 (30 min)	81	11
AB (AB 113 anionic) (pH 9.7)	18	12	Yes	No	Not Applicable	Not Applicable	56	26

Fig. 12 Summary of the results obtained from the competing processes during dye photodiscoloration using the α/β-Bi$_2$O$_3$ composite. The value of the degradation and the final TOC value were estimated correcting the initial concentration according to the percentage of adsorption for each dye.

measurements of the absorbance spectra were used to monitor the photolysis (% C_{photo}) and the photodegradation (% C_{deg}) using UV and visible irradiation, while the adsorption–desorption equilibrium was evaluated in the dark. In order to distinguish photodegradation from photobleaching, the theoretical absorbance spectra of the leuco-dye forms and the degradation products were calculated and compared with the experimental data. For the three dyes used, photodegradation was observed; therefore, using a non-spectrophotometric technique, we proceeded to estimate the percentage of decrease of the total organic carbon (% C_n^{TOC}).

The results are summarized in Fig. 12, where the percentage of photodegradation (% C_{deg}), the TOC decrease (% C_n^{TOC}) and the mineralization (% Mine) are reported. Moreover, based on the analysis of the spectrum and the response under UV/visible light, we concluded that for the AB dye, the results can be influenced by sensitization and eqn (1) cannot be applied. Therefore, for the AB dye, estimations of the percentage of degradation and reaction rate will be misleading.

The reported % C_{deg} are absolute values corrected according to the effective initial concentration (C_1); this was not falsified by the adsorption, as has been observed in many other studies.[46,53–55,91] By this, we do not mean that adsorption is not essential, because it is known that photoinduced reactions occur on the surface and, therefore, the adsorption of dye molecules on the photocatalyst is a requirement for photodegradation. However, as C_1 decreases, the % C_{deg} along with the efficiency of the photocatalyst increase.[20] Thus, comparison of the % C_{deg} values of different samples requires similar C_1 values (equal C_0 values is not enough). Otherwise, the material with the larger θ_{ads} will be falsely selected as the best photocatalyst because it shows a larger decrease in both the absorbance and the TOC due to the lower initial concentration of probe-molecules in solution. For example, Basu et al.[5] compared the visible light photodegradation of methylene blue solutions using ZnO and ZnO/CuS nanostructures using the same initial concentration (C_0). However, 72% of the dye was adsorbed on the ZnO/CuS in the dark, while no adsorption was observed for the ZnO. Although the authors measured the adsorption in the dark, no corrections were applied to estimate the percentage of photodegradation; therefore, they concluded that the ZnO/CuS nanostructures performed better, although a proper estimation would provide marginal differences. A similar analysis comparing Ag_3PO_4 and bentonite-supported Ag_3PO_4 (EB-Ag_3PO_4) photocatalysts was reported by Ma et al.[62] The authors reported that the RhB degradation by the EB-Ag_3PO_4 composite reached about 95% discoloration under visible light irradiation, which was much higher than that of Ag_3PO_4 (82%) for the same irradiation time; however, the difference in the dark-adsorption was much larger (50% for EB-Ag_3PO_4 in comparison to 15% for Ag_3PO_4). In such a case, it is not appropriate to conclude that the activity of the supported catalyst was enhanced, as the authors did. This adsorption/degradation mechanism has been reported by different authors[92–99] as a synergistic decontamination method.

However, herein, we are concerned with selecting a semiconductor material or a heterojunction as a good photocatalyst in which the organic molecule is mineralized by the action of sunlight, not adsorbed. Adsorption is clearly important; however, because there is a strong dependence of the photodegradation kinetic rate on the initial pollutant concentration,[81,100–102] comparisons between different materials should be performed at similar initial pollutant concentrations.[103]

In addition to the correct estimation of the adsorption, our results suggest that quantum chemical calculations provide useful information about the degradation or discoloration pathways of dyes of interest. It was shown that IC is a good probe molecule because photobleaching and photodegradation can be clearly distinguished by changes in the spectrum and IC intermediates are easily identified. Meanwhile, for RhB, the distinction between photobleaching and photodegradation requires further experiments; however, it can provide spectral information about sensitization. Finally, AB is not recommended for photocatalysis experiments due to the large number of intermediates whose absorbances interfere with the AB absorbance.

Deep understanding of the reactions involved during photodegradation and mineralization processes requires other measurements, such as the direct detection of ˙OH free radicals,[87] the use of hole, electron and radical scavengers[104,105] and, from the point of view of materials, the determination of the conduction and valence band positions relative to the standard redox potentials of the adsorbed species.[32] Here, we only propose a methodology to perform a proper assessment of the potential photocatalytic activity of a semiconductor material.

From a practical point of view, the aim of wastewater treatment is to diminish its ecological impact by decreasing the light absorption (color removal) and/or inhibiting the toxicity of residual molecules to living organisms. Therefore, after photodiscoloration, evaluation of the total mineralization is important. When the degradation of the parent pollutants and their intermediate compounds into CO_2 and H_2O is not complete and some residual contaminants remain in the water, it is necessary to assess the potential ecological and health risks of the degradation products.

Conclusions

The main conclusions from this work are summarized in Fig. 13, where we propose a methodology for the proper evaluation of the photocatalytic properties of semiconductors using standard techniques such as spectrophotometric and TOC analysis.

By following this methodology, it is possible to reach correct conclusions about the photocatalytic activity of a material without relying only on the decrease of the absorbance (A_{max}). As described above, the absorbance reduction can be due to either photodegradation of the molecules or to other non-photocatalytic processes (photobleaching, photolysis,

This journal is © The Royal Society of Chemistry 2019

Catal. Sci. Technol., 2019, 9, 1476–1496 | 1491

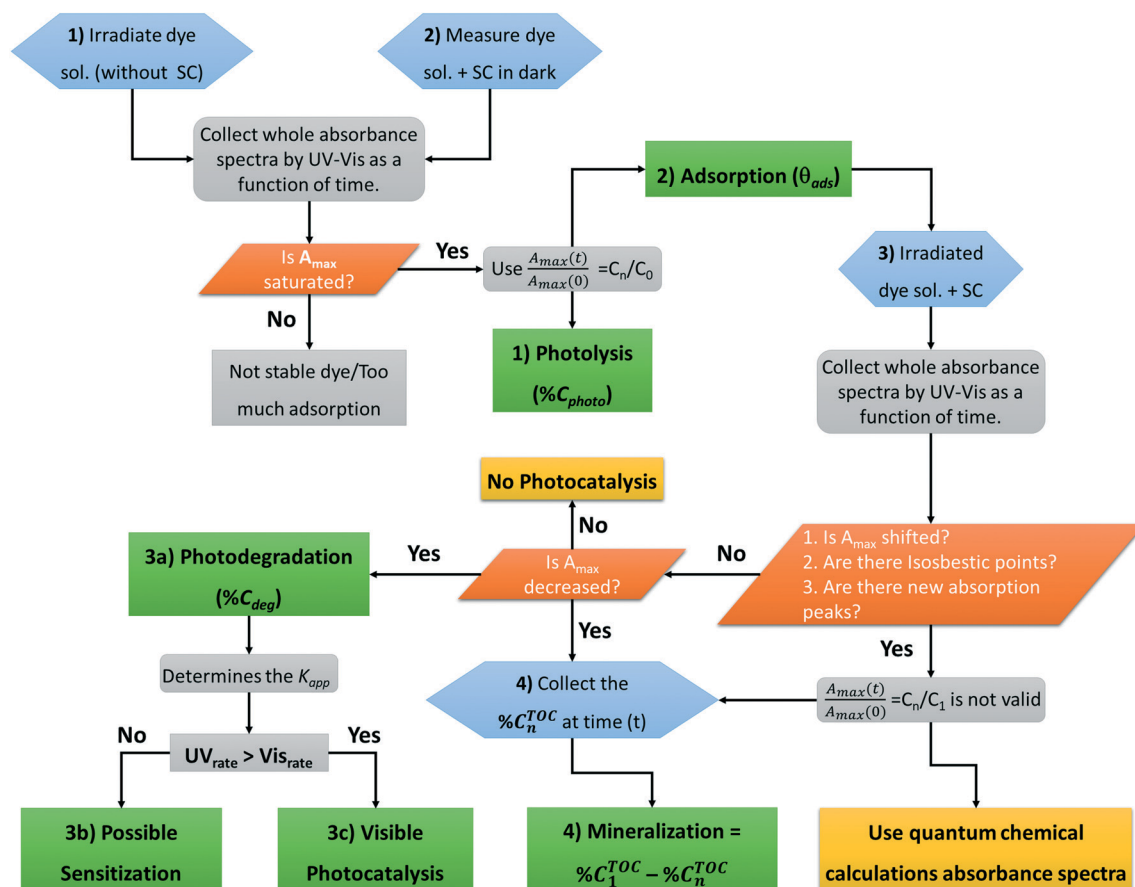## Flow diagram for the absorbance spectral analysis

Fig. 13 Proposed flow diagram for the photocatalytic evaluation of semiconductors. Numbers indicate the experiment to perform (hexagons) and the corresponding information achieved for each experiment (rectangles). SC refers to the semiconductor material either as a powder or a thin film.

sensitization). From the analysis, we conclude that all four processes discussed are important; however, adsorption appears to be the most critical because it is larger and although it is commonly measured, it is not properly quantified as a non-photocatalytic process. Adsorption should be measured in the dark at different initial concentrations and under the exact experimental conditions (pH, photocatalyst load, stirring rate) of the photodegradation experiments. We suspect that many of the misunderstandings about the photocatalytic activity of semiconductors using dyes as test molecules may arise from neglecting the degree of adsorption because this leads to errors in the effective initial concentration of the dye, which invalidates comparisons between different materials or probe-molecules. Sensitization can be identified by comparing the response of the material using illuminations that are resonant and non-resonant with the electronic absorption of the molecule. Additionally, we propose the use of quantum chemical calculations to distinguish between photobleaching and photodegradation but also to identify the contribution of possible degradation products to the absorbance spectra.

The degradation of the molecule is initiated with the molecular cleavage of the chromophore group due to interactions with the reactive oxygen species (superoxides, hydroxyl radicals or holes) and is identified by a decrease in the maximum absorbance. However, for some molecules, the degradation products or intermediates absorb light in the same spectral region; thus, it is impossible to make a correlation between the absorbance and concentration of the dye in solution. This effect is usually neglected because only the maximum value is recorded. The methodology proposed here, which is based on experimental–theoretical analysis, requires the acquisition and analysis of entire absorbance spectra.

Finally, to distinguish between photodegradation and photodiscoloration and to determine the degree of mineralization, it is necessary to perform quantification of the total organic carbon in solution by an independent technique. The degree of mineralization must be corrected by considering the fraction of adsorbed molecules.

The example material chosen here to illustrate the methodology is the $\alpha/\beta\text{-Bi}_2\text{O}_3$ heterostructure; according to the

spectrophotometric response, it appears to be very effective for the three dyes. However, a careful revision of the evolution of the absorption spectra and the TOC decrease indicated that this material has low photocatalytic activity for water treatment. The conclusion should be that based on the lower values of % Mine obtained by TOC in comparison to the estimated $% C_{deg}$ inferred from the absorbance spectra, the tested semiconductor (α/β-Bi$_2$O$_3$) is very effective to induce photodiscoloration of the dye molecules; however, the intermediate products remain in solution without degradation.

Author contributions

The manuscript was written through contributions of all authors. All authors have given approval to the final version of the manuscript.

Funding sources

Nomenclature

A	Absorbance according to the Beer–Lambert law ($A = \varepsilon\, l\, C$)
AB	Acid blue 113 dye
A–D	Adsorption–desorption equilibrium
A_{max}	Maximum absorbance value of the probe-molecule measured at a fixed wavelength
A_{max}^*	Maximum absorbance value of the intermediate products measured at a fixed wavelength
C_n	Concentration of dye in solution acquired from A_{max}
$C(t)$	Concentration of the probe-molecule in solution at a specific time of irradiation
C_0	Initial concentration of the probe-molecule in solution (equal to unity)
C_1	Concentration of the probe-molecule in solution after adsorption–desorption equilibrium
C_{ads}	Relative concentration (C/C_0) of the probe-molecule after the adsorption process
C_{photo}	Relative concentration (C/C_0) of the probe-molecule after the photolysis process
C_{deg}	Relative concentration (C/C_1) of the probe-molecule after the photodegradation process using the photocatalyst material
C_{TOC}	Concentration of the probe-molecule after the photodegradation process using TOC analysis
$% C_0^{TOC}$	Total organic carbon of the original dye solution, equal to 100%
$% C_1^{TOC}$	Theoretical or experimental effective total organic carbon of the dye solution
$% C_n^{TOC}$	Total organic carbon of the irradiated dye solution by TOC analysis
$% C_{photo}$	Percentage of degradation of the probe-molecule by the photolysis process
$% C_{disc}$	Percentage of discoloration of the probe-molecule by the photocatalytic process
$% C_{deg}$	Percentage of degradation of the probe-molecule by the photocatalytic process
% Mine	Percentage of mineralization of the probe-molecule by the photocatalytic process calculated by the TOC analysis value
IC	Indigo carmine dye
I_i	Concentration of intermediate products formed from dye degradation
K_{app}	Apparent kinetic rate constant of the photodegradation of the probe-molecule
k_r	Rate constant of the photodegradation of the probe-molecule
K_S	Adsorption constant of the probe-molecule
K_{Si}	Adsorption constant of intermediate products formed from dye degradation
L–H	Langmuir–Hinshelwood
PZC	Point of zero charge of a material
r	Rate of the reaction during the photocatalytic process
RhB	Rhodamine-B dye
ROS	Reactive oxygen species
S	Sensitization of the organic molecule by light
SMD	Solvation model based on density
TD-DFT	Time-dependent-density functional theory
TOC	Total organic carbon
ε	Absorptivity coefficient of the organic molecule
λ	Fixed wavelength of the absorbance of the dye
λ_{max}	Wavelength of A_{max} of each probe-molecule
θ_{ads}	Fraction of probe-molecules adsorbed on the photocatalyst surface
$% \theta_{ads}^{TOC}$	Total organic carbon calculated from the fraction of probe-molecules adsorbed on the photocatalyst surface

Conflicts of interest

There are no conflicts to declare.

Acknowledgements

DGTIC of UNAM for their excellent and free supercomputing services.

References

1 D. F. Oliveira, P. S. Batista, P. S. Muller, V. Velani, M. D. França, D. R. De Souza and A. E. Machado, *Dyes Pigm.*, 2012, **92**, 563–572.

2 S. Bagheri, A. TermehYousefi and T.-O. Do, *Catal. Sci. Technol.*, 2017, 7, 4548–4569.

3 M. Rochkind, S. Pasternak and Y. Paz, *Molecules*, 2014, **20**, 88–110.

4 J.-M. Herrmann, *Catal. Today*, 1999, **53**, 115–129.

5 M. Basu, N. Garg and A. K. Ganguli, *J. Mater. Chem. A*, 2014, **2**, 7517–7525.

6 C. P. Ireland, R. G. Palgrave, S. C. Bennett, A. W. J. Smith, J. H. Clark, J. R. Darwent, J. B. Claridge, S. Poulston and M. J. Rosseinsky, *J. Mater. Chem. A*, 2016, **4**, 12479–12486.

7 L. Li, J. Deng, R. Yu, J. Chen, Z. Wang and X. Xing, *J. Mater. Chem. A*, 2013, **1**, 11894–11900.

8 L. Mohapatra and K. Parida, *J. Mater. Chem. A*, 2016, **4**, 10744–10766.

9 I. K. Konstantinou and T. A. Albanis, *Appl. Catal., B*, 2004, **49**, 1–14.

10 N. M. Mahmoodi, M. Arami, N. Y. Limaee and N. S. Tabrizi, *Chem. Eng. J.*, 2005, **112**, 191–196.

11 F. M. D. Chequer, D. P. de Oliveira, E. R. A. Ferraz, G. A. R. de Oliveira, J. C. Cardoso and M. V. B. Zanoni, *Textile dyes: dyeing process and environmental impact*, INTECH Open Access Publisher, 2013.

12 H. Lachheb, E. Puzenat, A. Houas, M. Ksibi, E. Elaloui, C. Guillard and J.-M. Herrmann, *Appl. Catal., B*, 2002, **39**, 75–90.

13 M. A. Rauf and S. S. Ashraf, *Chem. Eng. J.*, 2009, **151**, 10–18.

14 M. Vautier, C. Guillard and J.-M. Herrmann, *J. Catal.*, 2001, **201**, 46–59.

15 B. Ohtani, *Phys. Chem. Chem. Phys.*, 2014, **16**, 1788–1797.

16 K. Rajeshwar, M. E. Osugi, W. Chanmanee, C. R. Chenthamarakshan, M. V. B. Zanoni, P. Kajitvichyanukul and R. Krishnan-Ayer, *J. Photochem. Photobiol., C*, 2008, **9**, 171–192.

17 J.-M. Herrmann, *Appl. Catal., B*, 2010, **99**, 461–468.

18 A. V. Emeline, V. K. Ryabchuk and N. Serpone, *J. Phys. Chem. B*, 2005, **109**, 18515–18521.

19 N. Barbero and D. Vione, *Environ. Sci. Technol.*, 2016, **50**, 2130–2131.

20 S. Bae, S. Kim, S. Lee and W. Choi, *Catal. Today*, 2014, **224**, 21–28.

21 T. A. Gadhi, A. Hernández-Gordillo, M. Bizarro, P. Jagdale, A. Tagliaferro and S. E. Rodil, *Ceram. Int.*, 2016, **42**, 13065–13073.

22 G. W. T. M. J. Frisch, H. B. Schlegel, G. E. Scuseria, M. A. Robb, J. R. Cheeseman, J. J. A. Montgomery, T. Vreven, K. N. Kudin, J. C. Burant, J. M. Millam, S. S. Iyengar, J. Tomasi, V. Barone, B. Mennucci, M. Cossi, G. Scalmani, N. Rega, G. A. Petersson, H. Nakatsuji, M. Hada, M. Ehara, K.

Toyota, R. Fukuda, J. Hasegawa, M. Ishida, T. Nakajima, Y. Honda, O. Kitao, H. Nakai, M. Klene, X. Li, J. E. Knox, H. P. Hratchian, J. B. Cross, V. Bakken, C. Adamo, J. Jaramillo, R. Gomperts, R. E. Stratmann, O. Yazyev, A. J. Austin, R. Cammi, C. Pomelli, J. W. Ochterski, P. Y. Ayala, K. Morokuma, G. A. Voth, P. Salvador, J. J. Dannenberg, V. G. Zakrzewski, S. Dapprich, A. D. Daniels, M. C. Strain, O. Farkas, D. K. Malick, A. D. Rabuck, K. Raghavachari, J. B. Foresman, J. V. Ortiz, Q. Cui, A. G. Baboul, S. Clifford, J. Cioslowski, B. B. Stefanov, G. Liu, A. Liashenko, P. Piskorz, I. Komaromi, R. L. Martin, D. J. Fox, T. Keith, M. A. Al-Laham, C. Y. Peng, A. Nanayakkara, M. Challacombe, P. M. W. Gill, B. Johnson, W. Chen, M. W. Wong, C. Gonzalez and J. A. Pople, *Gaussian 09*, Revision A.08 Inc., 2009.

23 Y. Zhao, N. E. Schultz and D. G. Truhlar, *J. Chem. Phys.*, 2005, **123**, 161103.

24 G. A. Petersson and M. A. Al-Laham, *J. Chem. Phys.*, 1991, **94**, 6081–6090.

25 G. A. Petersson, A. Bennett, T. G. Tensfeldt, M. A. Al-Laham, W. A. Shirley and J. Mantzaris, *J. Chem. Phys.*, 1988, **89**, 2193–2218.

26 A. D. McLean and G. S. Chandler, *J. Chem. Phys.*, 1980, **72**, 5639–5648.

27 R. Krishnan, J. S. Binkley, R. Seeger and J. A. Pople, *J. Chem. Phys.*, 1980, **72**, 650–654.

28 A. V. Marenich, C. J. Cramer and D. G. Truhlar, *J. Phys. Chem. B*, 2009, **113**, 6378–6396.

29 E. Runge and E. K. U. Gross, *Phys. Rev. Lett.*, 1984, **52**, 997–1000.

30 M. E. Casida, H. Chermette and D. Jacquemin, *J. Mol. Struct.: THEOCHEM*, 2009, **914**, 1–2.

31 F. Santoro and D. Jacquemin, *Wiley Interdiscip. Rev.: Comput. Mol. Sci.*, 2016, **6**, 460–486.

32 Y. Xu and M. A. A. Schoonen, *American Mineralogist*, 2000, vol. 85, pp. 543–556.

33 S. S. Youji Li, M. Ma, Y. Ouyang and W. Yan, *Chem. Eng. J.*, 2008, **142**, 147–155.

34 J. Zhang and Y. Nosaka, *J. Phys. Chem. C*, 2013, **117**, 1383–1391.

35 Q. Xiang, J. Yu and P. K. Wong, *J. Colloid Interface Sci.*, 2011, **357**, 163–167.

36 H. Guan, L. Zhu, H. Zhou and H. Tang, *Anal. Chim. Acta*, 2008, **608**, 73–78.

37 N. G. Asenjo, R. Santamaría, C. Blanco, M. Granda, P. Álvarez and R. Menéndez, *Carbon*, 2013, **55**, 62–69.

38 D. F. Ollis, *J. Phys. Chem. B*, 2005, **109**, 2439–2444.

39 Z. Khuzwayo and E. M. N. Chirwa, *J. Hazard. Mater.*, 2015, **300**, 459–466.

40 N. S. a. A. V. Emeline, *Int. J. Photoenergy*, 2002, **4**, 91–131.

41 K. B. Fontana, G. G. Lenzi, E. C. R. Seára and E. S. Chaves, *Ecotoxicol. Environ. Saf.*, 2018, **151**, 127–131.

42 Y. Kohno, S. Kitamura, T. Yamada, K. Sugihara and S. Ohta, *Life Sci.*, 2005, **77**, 601–614.

43 J.-X. Ma, H. Yang, S. Li, R. Ren, J. Li, X. Zhang and J. Ma, *RSC Adv.*, 2015, **5**, 97520–97527.

44 K. Gude, V. M. Gun'ko and J. P. Blitz, *Colloids Surf., A*, 2008, **325**, 17–20.

1494 | *Catal. Sci. Technol.*, 2019, **9**, 1476–1496

This journal is © The Royal Society of Chemistry 2019

45 V. Etacheri, R. Roshan and V. Kumar, *ACS Appl. Mater. Interfaces*, 2012, **4**, 2717–2725.

46 H.-Y. Xu, L.-C. Wu, H. Zhao, L.-G. Jin and S.-Y. Qi, *PLoS One*, 2015, **10**, e0142616.

47 S. Merouani, O. Hamdaoui, F. Saoudi and M. Chiha, *Chem. Eng. J.*, 2010, **158**, 550–557.

48 A. G. S. Prado, L. B. Bolzon, C. P. Pedroso, A. O. Moura and L. L. Costa, *Appl. Catal., B*, 2008, **82**, 219–224.

49 S. Mohammadzadeh, M. E. Olya, A. M. Arabi, A. Shariati and M. R. K. Nikou, *J. Environ. Sci.*, 2015, **35**, 194–207.

50 E. Kordouli, K. Bourikas, A. Lycourghiotis and C. Kordulis, *Catal. Today*, 2015, **252**, 128–135.

51 J. Xiao, H. Zhang, Y. Xia, Z. Li and W. Huang, *RSC Adv.*, 2016, **6**, 39861–39869.

52 K. Tanaka, K. Padermpole and T. Hisanaga, *Water Res.*, 2000, **34**, 327–333.

53 L. Shan, G. Wang, D. Li, X. San, L. Liu, L. Dong and Z. Wu, *Dalton Trans.*, 2015, **44**, 7835–7843.

54 S. Ghosh, N. A. Kouamé, L. Ramos, S. Remita, A. Dazzi, A. Deniset-Besseau, P. Beaunier, F. Goubard, P.-H. Aubert and H. Remita, *Nat. Mater.*, 2015, **14**, 505.

55 S. Wang, Y. Zhang, T. Zhang, F. Dong and H. Huang, *Readily attainable spongy foam photocatalyst for promising practical photocatalysis*, 2017.

56 J. Piella, F. Merkoci, A. Genc, J. Arbiol, N. G. Bastus and V. Puntes, *J. Mater. Chem. A*, 2017, **5**, 11917–11929.

57 T. Bechtold, A. Turcanu, S. Geissler and E. Ganglberger, *Bioresour. Technol.*, 2002, **81**, 171–177.

58 N. Srividya, G. Paramasivan, K. Seetharaman and P. Ramamurthy, *J. Chem. Soc., Faraday Trans.*, 1994, **90**, 2525–2530.

59 A. Hernández-Gordillo, V. Rodríguez-González, S. Oros-Ruiz and R. Gómez, *Catal. Today*, 2016, **266**, 27–35.

60 C. Pan, J. Xu, Y. Chen and Y. Zhu, *Appl. Catal., B*, 2012, **115–116**, 314–319.

61 R. Pol, M. Guerrero, E. García-Lecina, A. Altube, E. Rossinyol, S. Garroni, M. D. Baró, J. Pons, J. Sort and E. Pellicer, *Appl. Catal., B*, 2016, **181**, 270–278.

62 J. Ma, Q. Liu, L. Zhu, J. Zou, K. Wang, M. Yang and S. Komarneni, *Appl. Catal., B*, 2016, **182**, 26–32.

63 Z. Wu, X. Yuan, G. Zeng, L. Jiang, H. Zhong, Y. Xie, H. Wang, X. Chen and H. Wang, *Appl. Catal., B*, 2018, **225**, 8–21.

64 N. U. Silva, T. G. Nunes, M. S. Saraiva, M. S. Shalamzari, P. D. Vaz, O. C. Monteiro and C. D. Nunes, *Appl. Catal., B*, 2012, **113–114**, 180–191.

65 S. Rasalingam, R. Peng and R. T. Koodali, *Appl. Catal., B*, 2015, **174–175**, 49–59.

66 G. Liu and J. Zhao, *New J. Chem.*, 2000, **24**, 411–417.

67 X. Lang, X. Chen and J. Zhao, *Chem. Soc. Rev.*, 2014, **43**, 473–486.

68 R. Camarillo and J. Rincón, *Chem. Eng. Technol.*, 2011, **34**, 1675–1684.

69 D. Chatterjee and A. Mahata, *J. Photochem. Photobiol., A*, 2002, **153**, 199–204.

70 T. Watanabe, T. Takizawa and K. Honda, *J. Phys. Chem.*, 1977, **81**, 1845–1851.

71 S.-K. Lee, A. Mills and C. O'Rourke, *Chem. Soc. Rev.*, 2017, **46**, 4877–4894.

72 R. Quesada-Cabrera, A. Mills and C. O'Rourke, *Appl. Catal., B*, 2014, **150–151**, 338–344.

73 W. Kuo and P. Ho, *Chemosphere*, 2001, **45**, 77–83.

74 R. Su, R. Tiruvalam, Q. He, N. Dimitratos, L. Kesavan, C. Hammond, J. A. Lopez-Sanchez, R. Bechstein, C. J. Kiely and G. J. Hutchings, *ACS Nano*, 2012, **6**, 6284–6292.

75 B. Liu, X. Zhao, C. Terashima, A. Fujishima and K. Nakata, *Phys. Chem. Chem. Phys.*, 2014, **16**, 8751–8760.

76 S. Sarkar, R. Das, H. Choi and C. Bhattacharjee, *RSC Adv.*, 2014, **4**, 57250–57266.

77 F. Chen, J. Zhao and H. Hidaka, *Int. J. Photoenergy*, 2003, **5**, 209–217.

78 X. Hu, T. Mohamood, W. Ma, C. Chen and J. Zhao, *J. Phys. Chem. B*, 2006, **110**, 26012–26018.

79 Z. Youssef, L. Colombeau, N. Yesmurzayeva, F. Baros, R. Vanderesse, T. Hamieh, J. Toufaily, C. Frochot, T. Roques-Carmes and S. Acherar, *Dyes Pigm.*, 2018, **159**, 49–71.

80 H. Liu, N. Gao, M. Liao and X. Fang, *Sci. Rep.*, 2015, **5**, 7716.

81 G. Cinelli, F. Cuomo, L. Ambrosone, M. Colella, A. Ceglie, F. Venditti and F. Lopez, *Journal of Water Process Engineering*, 2017, **20**, 71–77.

82 M. M. Sousa, C. Miguel, I. Rodrigues, A. J. Parola, F. Pina, J. S. S. de Melo and M. J. Melo, *Photochem. Photobiol. Sci.*, 2008, **7**, 1353–1359.

83 M. Coelho, F. de Andrade, G. de Lima, R. Augusti, M. Ferreira, D. Maria and J. Ardisson, *Appl. Organomet. Chem.*, 2011, **25**, 220–225.

84 M. Coelho, G. De Lima, R. Augusti, D. Maria and J. Ardisson, *Appl. Catal., B*, 2010, **96**, 67–71.

85 I. Dalmázio, A. P. F. M. de Urzedo, T. M. A. Alves, R. R. Catharino, M. N. Eberlin, C. C. Nascentes and R. Augusti, *J. Mass Spectrom.*, 2007, **42**, 1273–1278.

86 H. Liu, A. Imanishi and Y. Nakato, *J. Phys. Chem. C*, 2007, **111**, 8603–8610.

87 J. Zhang and Y. Nosaka, *J. Phys. Chem. C*, 2013, **117**, 1383–1391.

88 K.-i. Ishibashi, A. Fujishima, T. Watanabe and K. Hashimoto, *Electrochem. Commun.*, 2000, **2**, 207–210.

89 Q. Xiang, J. Yu and P. K. Wong, *J. Colloid Interface Sci.*, 2011, **357**, 163–167.

90 D. Sánchez-Martínez, I. Juárez-Ramírez, L. M. Torres-Martínez and I. de León-Abarte, *Ceram. Int.*, 2016, **42**, 2013–2020.

91 M.-S. Gui, W.-D. Zhang, Q.-X. Su and C.-H. Chen, *J. Solid State Chem.*, 2011, **184**, 1977–1982.

92 A. Sandoval, C. Hernández-Ventura and T. E. Klimova, *Fuel*, 2017, **198**, 22–30.

93 M. Zhao, Q. Yuan, H. Zhang, C. Li, Y. Wang and W. Wang, *J. Alloys Compd.*, 2019, **782**, 1049–1057.

94 J. Lyu, Z. Hu, Z. Li and M. Ge, *J. Phys. Chem. Solids*, 2019, **129**, 61–70.

This journal is © The Royal Society of Chemistry 2019

Catal. Sci. Technol., 2019, **9**, 1476–1496 | **1495**

95 O. Sacco, M. Matarangolo, V. Vaiano, G. Libralato, M. Guida, G. Lofrano and M. Carotenuto, *Sci. Total Environ.*, 2018, **644**, 430–438.

96 X. Wang, J. Zhou, S. Zhao, X. Chen and Y. Yu, *Appl. Surf. Sci.*, 2018, **453**, 394–404.

97 X. Bing, X. Jian, J. Chu, J. Li and C. Guo, *Mater. Res. Bull.*, 2019, **110**, 1–12.

98 S. K. Mandal, K. Dutta, S. Pal, S. Mandal, A. Naskar, P. K. Pal, T. S. Bhattacharya, A. Singha, R. Saikh, S. De and D. Jana, *Mater. Chem. Phys.*, 2019, **223**, 456–465.

99 S. Jiao, Y. Zhao, C. Li, B. Wang and Y. Qu, *Green Energy & Environment*, 2019, **4**, 66–74.

100 F. Venditti, F. Cuomo, A. Ceglie, P. Avino, M. V. Russo and F. Lopez, *Langmuir*, 2015, **31**, 3627–3634.

101 K. Wetchakun, N. Wetchakun and S. Sakulsermsuk, *J. Ind. Eng. Chem.*, 2019, **71**, 19–49.

102 C.-H. Wu, H.-W. Chang and J.-M. Chern, *J. Hazard. Mater.*, 2006, **137**, 336–343.

103 A. Chakraborty, D. A. Islam and H. Acharya, *J. Solid State Chem.*, 2019, **269**, 566–574.

104 C.-Y. Chu and M. H. Huang, *J. Mater. Chem. A*, 2017, **5**, 15116–15123.

105 D. Wang, L. Guo, Y. Zhen, L. Yue, G. Xue and F. Fu, *J. Mater. Chem. A*, 2014, **2**, 11716–11727.